A comparison of lattice Boltzmann schemes for sub-critical shallow water flows

DOI:
10.1063/5.0147175

Document Version
Accepted author manuscript

Accepted to Phys. Fluids 10.1063/5.0147175

A comparison of lattice Boltzmann schemes for sub-critical shallow water flows

Alessandro De Rosis[1, a)]
Department of Mechanical, Aerospace and Civil Engineering, The University of Manchester, Manchester M13 9PL, UK

In this paper, we test the numerical properties of several variants of the lattice Boltzmann method (LBM) for simulating the shallow water flows. Specifically, we perform a systematic comparison of five different schemes: (i) the single-relaxation-time LBM, the (ii) raw-moments-based and (iii) central-moments-based multiple-relaxation-time LBMs, the (iv) two-stages and (v) one-stage simplified LBMs. Concerning the latter, traditional simplified schemes require a fractional step two-stages technique. Building on the work A. Delgado-Gutiérrez, P. Marzocca, D. Cárdenas, and O. Probst, "A single-step and simplified graphics processing unit lattice Boltzmann method for high turbulent flows," Int J Numer Meth Fl 93, 2339–2361, we derive a one-stage approach, where the procedure spans the grid points just once per time step. All the aforementioned LBMs are tested against five well-consolidated benchmark problems and their numerical performance is assessed. Overall, populations-based schemes show superior accuracy and convergence properties. We link this behaviour to the higher numerical dissipation introduced by the simplified models.

Keywords: Lattice Boltzmann method, shallow water equations, dam break

I. INTRODUCTION

A shallow water flow occurs when the fluid depth is substantially smaller than the flow horizontal length scales. In this case, the flow can be approximated by the shallow water equations, which are a set of partial differential equations that explain the fluid behaviour[1]. Atmospheric flows[2] and oceanic currents[3] are only few examples of the numerous phenomena that may occur when shallow water moves. The water flow in rivers and other waterways can be modelled using the SWEs. This can be helpful for anticipating and planning for floods, which can seriously harm infrastructure and communities[4]. Moreover, the behaviour at coastlines may be unpredictable and complex. The interactions between waves, currents, and tides can be modelled using the SWEs, which can assist engineers in creating buildings that are more resistant to erosion and other coastal dangers[5]. In addition, large, catastrophic waves known as tsunamis caused by earthquakes or other geological occurrences can be modelled using the SWEs, which can aid in community planning and response[6]. The shallow water equations are obtained by integrating the Navier-Stokes ones over the fluid depth[7] and can be solved numerically by adopting different techniques. For instance, Casulli[8] proposed a semi-implicit finite-differences scheme. Toro[9] assessed the properties of the weighted average flux method. Finite-volumes methods were developed by Zhou[10], who performed a SIMPLE-like implementation, and Alcrudo & Garcia-Navarro[11], who successfully tested a high-order Godunov-type scheme against rapidly varying inviscid shallow water flows.

All the aforementioned approaches require the solution of the macroscopic governing SWEs. A different viewpoint is offered by the lattice Boltzmann method, that is a reliable alternative to perform fluid flow simulations[12,13]. In short, the LBM idealises the fluid as collections (also known as distributions or populations) of fictitious particles moving along the links of a fixed Cartesian lattice. The macroscopic behaviour stems from the moments of these distributions. If compared to traditional methods for computational fluid dynamics, it possesses some very attractive features, *e.g.* algorithmic simplicity, high computational efficiency and great flexibility in dealing with complex physics[14]. The LBM has been widely applied to simulate phenomena governed by the Navier-Stokes equations for incompressible flows[15]. However, many efforts demonstrated that it can be successfully employed to recover other classes of partial differential equations, ranging from advection-diffusion processes[16] to the spread of epidemics[17]. Interestingly, a compelling example is represented by solution of the the shallow water equations. Zhou proposed seminal contributions[18–20] by deriving a single-relaxation-time BGK LBM able to recover the solution of the SWEs. Building on this work, many studies developed in this field, focussing for example on turbulent transient flows[21] and multi-layer models[22–25]. Despite its wide popularity, the BGK collision operator is known to be prone to numerical instability due to the presence of non-hydrodynamic ghost modes[26]. Indeed, Dellar[27] demonstrated the existence of an instability in the BGK LBM for shallow water equations. By decomposing the collision stage on a basis of raw moments, the multiple-relaxation-time model can successfully damp high-order non-hydrodynamic modes[28,29] and increase the stability of the algorithm. An MRT model for the SWEs was proposed in Refs.[30,31], showing superior stability properties with respect to the BGK LBM. However, the MRT breaks the Galilean invariance due to the representation of the collision in a frame at rest[32]. A solution to this issue is presented by performing the collision in the space of central moments[33,34]. Interestingly,

a)Electronic mail: alessandro.derosis@manchester.ac.uk

many efforts elucidated the excellent numerical properties of this approach[35–38].

Single- and multiple-relaxation-time LBMs involve the computation and storage of the particle distribution functions at each grid point. Unfortunately, it may lead to a very high demand of virtual memory, especially if dense resolutions are necessary to capture the presence of fine flow features. In fact, by adopting the nine-velocities discretization[12], the typical simulation has to store (at least) nine values per grid point. In contrast to populations-based approaches, the simplified lattice Boltzmann method[39–45] avoids the computation of the space-time evolution of the particle distribution functions and involves only macroscopic variables. In the case of shallow water flows, the SLBM has to only deal with the water height and the two components of the flow velocity vector. Hence, the SLBM demands to compute and store only these quantities at each lattice site, while the computation and storage of populations are completely disregarded. As a consequence, the amount of requested virtual memory reduces. The SLBM algorithm is built on a fractional step technique, where the typical time step is split into two stages: predictor and corrector. In a recent effort, Maquignon *et al.*[46] successfully presented an attempt to recover the solution of the SWEs. Interestingly, Delgado-Gutiérrez *et al.*[47] proposed a one-stage SLBM to recover the solution of the Navier-Stokes equations, that needs to span the nodes just once per time step. Very recently, De Rosis *et al.*[48] derived an SSLBM for magnetohydrodynamic flows, where they proved that the SSLBM is able to alleviate the excessive numerical diffusion of the SLBM[49].

In this work, we perform a quantitative assessment and comparison of five schemes for the simulation of shallow water flows: (i) single-relaxation-time LBM[18], (ii) raw-moments-based multiple-relaxation-time LBM, (iii) central-moments-based multiple-relaxation-time LBM[50], (iv) SLBM[46] and (v) SSLBM. The latter is an original contribution of this work and represents an extension of the work done by Delgado-Gutiérrez *et al.*[47] to SWEs. The numerical properties of these five schemes are tested against five well-defined, consolidated and popular benchmark tests. Some considerations about the virtual memory usage are drawn too. While our numerical analyses focus on sub-critical flows (*i.e.*, the Froude number is less than 1), it is worth to mention that super-critical flows are an actual challenge for LBM simulations. The interested reader can refer to Refs.[51,52] for additional details about super-critical flows, that do not represent the scope of the present manuscript.

The rest of the paper is organized as follows. In Sec. II, the methodologies are devised. Results from our numerical analyses are discussed in Sec. III. Eventually, some conclusions are drawn in Sec. IV.

II. LATTICE BOLTZMANN MODELLING OF SHALLOW WATER FLOWS

In this section, first the governing equations are stated. Secondly, the BGK LBM proposed in the seminal contribution by Zhou[18] is recalled. Thirdly, the central-moments-based scheme in Ref.[50] is discussed, together with its raw-moments-based counterpart. Fourthly, the two-stages simplified LBM in Ref.[46] is outlined. Eventually, our one-stage simplified scheme is described, together with the Chapman-Enskog expansion.

A. Macroscopic governing equations

By neglecting the vertical direction, let us consider a two-dimensional Cartesian reference system of axes $\mathbf{x} = (x, y)$. By assuming a frictionless bottom surface, the continuity and momentum equations can be written as

$$\partial_t h + \partial_\alpha \left(h u_\alpha\right) = 0, \tag{1}$$

$$\partial_t \left(h u_\alpha\right) + \partial_\beta \left(h u_\alpha u_\beta\right) = -g\partial_\alpha \left(\frac{h^2}{2}\right) + \nu\partial_\beta \left(h\partial_\beta u_\alpha\right) + F_\alpha, \tag{2}$$

where the flow velocity vector is $\boldsymbol{u} = [u_x, u_y]$ and the indexes α and β span the Cartesian axes. To account for the bed elevation, the force vector $\boldsymbol{F} = [F_x, F_y]$ is written as

$$F_\alpha = -gh\partial_\alpha z. \tag{3}$$

B. BGK LBM in Ref.[18]

To build an LBM for the SWEs, Zhou[18] adopted the D2Q9 velocity space, where the populations $f_i = [f_0, f_1, f_2, f_3, f_4, f_5, f_6, f_7, f_8]$ collide and stream on a fixed square grid along the generic link $i = 0 \ldots 8$ with velocity $\mathbf{c}_i = [c_{ix}, c_{iy}]$ defined as

$$c_{ix} = [0,\ 1,\ 0,\ -1,\ 0,\ 1,\ -1,\ -1,\ 1], \tag{4}$$

$$c_{iy} = [0,\ 0,\ 1,\ 0,\ -1,\ 1,\ 1,\ -1,\ -1]. \tag{5}$$

The BGK lattice Boltzmann equation reads as follows:

$$f_i(\boldsymbol{x} + \mathbf{c}_i, t+1) = f_i(\boldsymbol{x}, t) + \omega\left[f_i^{eq}(\boldsymbol{x}, t) - f_i(\boldsymbol{x}, t)\right] + 3w_i\mathbf{c}_i \cdot \boldsymbol{F}. \tag{6}$$

The weighting factors are $w_0 = 4/9$, $w_{1,2,3,4} = 1/9$ and $w_{5,6,7,8} = 1/36$. As usual, the LBE can be divided into two steps, *i.e.* collision:

$$f_i^\star(\boldsymbol{x}, t) = f_i(\boldsymbol{x}, t) + \omega\left[f_i^{eq}(\boldsymbol{x}, t) - f_i(\boldsymbol{x}, t)\right] + 3w_i\mathbf{c}_i \cdot \boldsymbol{F}, \tag{7}$$

and streaming:

$$f_i(\boldsymbol{x} + \mathbf{c}_i, t+1) = f_i^\star(\boldsymbol{x}, t). \tag{8}$$

The second term of the right-hand side of Eq. (7) is the BGK collision operator, that forces all the populations to relax with the same rate ω to a discrete local equilibrium that is defined as[18]

$$
\begin{aligned}
f_0^{eq} &= h - \frac{5}{6}gh^2 - \frac{2}{3}h\left(u_x^2+u_y^2\right), \\
f_{1\ldots4}^{eq} &= \frac{gh^2}{6} + \frac{h}{3}\boldsymbol{u}\cdot\mathbf{c}_i + \frac{h}{2}\left(\boldsymbol{u}\cdot\mathbf{c}_i\right)^2 - \frac{h}{6}\left(u_x^2+u_y^2\right), \\
f_{5\ldots8}^{eq} &= \frac{gh^2}{24} + \frac{h}{12}\boldsymbol{u}\cdot\mathbf{c}_i + \frac{h}{8}\left(\boldsymbol{u}\cdot\mathbf{c}_i\right)^2 - \frac{h}{24}\left(u_x^2+u_y^2\right).
\end{aligned}
\tag{9}
$$

Macroscopic variables are then available simply as

$$
h = \sum_i f_i, \qquad \boldsymbol{m} = \sum_i f_i \mathbf{c}_i, \tag{10}
$$

where the vector $\boldsymbol{m} = [m_x, m_y]$ is defined as $\boldsymbol{m} = h\boldsymbol{u}$.

C. Central-moments-based MRT LBM in Ref.[50]

In the work by De Rosis[50], the collision operator is projected onto a basis of central moments[53–55]. Post-collision populations are evaluated as

$$
\begin{aligned}
f_0^\star &= r_0^\star - r_3^\star + r_8^\star, \\
f_1^\star &= \frac{1}{2}\left(r_1^\star - r_7^\star - r_8^\star\right) + \frac{1}{4}\left(r_3^\star + r_4^\star\right), \\
f_2^\star &= \frac{1}{2}\left(r_2^\star - r_6^\star - r_8^\star\right) + \frac{1}{4}\left(r_3^\star - r_4^\star\right), \\
f_3^\star &= \frac{1}{2}\left(-r_1^\star + r_7^\star - r_8^\star\right) + \frac{1}{4}\left(r_3^\star + r_4^\star\right), \\
f_4^\star &= \frac{1}{2}\left(-r_2^\star + r_6^\star - r_8^\star\right) + \frac{1}{4}\left(r_3^\star - r_4^\star\right), \\
f_5^\star &= \frac{1}{4}\left(r_5^\star + r_6^\star + r_{7\star} + r_8^\star\right), \\
f_6^\star &= \frac{1}{4}\left(-r_5^\star + r_6^\star - r_{7\star} + r_8^\star\right), \\
f_7^\star &= \frac{1}{4}\left(r_5^\star - r_6^\star - r_{7\star} + r_8^\star\right), \\
f_8^\star &= \frac{1}{4}\left(-r_5^\star - r_6^\star + r_7^\star + r_8^\star\right).
\end{aligned}
\tag{11}
$$

Quantities $r_{0\ldots8}^\star$ are the post-collision raw moments of the particle distributions. These are computed as

$$
\begin{aligned}
r_0^\star &= k_0^\star, \\
r_1^\star &= hu_x, \\
r_2^\star &= hu_y, \\
r_3^\star &= k_3^\star + h\left(u_x^2+u_y^2\right), \\
r_4^\star &= k_4^\star + h\left(u_x^2-u_y^2\right), \\
r_5^\star &= k_5^\star + hu_xu_y, \\
r_6^\star &= \frac{1}{2}u_y\left(k_3^\star + k_4^\star\right) + 2u_xk_5^\star + k_6^\star + hu_x^2u_y, \\
r_7^\star &= \frac{1}{2}u_x\left(k_3^\star - k_4^\star\right) + 2u_yk_5^\star + k_7^\star + hu_xu_y^2, \\
r_8^\star &= \frac{1}{2}k_3^\star\left(u_x^2+u_y^2\right) - \frac{1}{2}k_4^\star\left(u_x^2-u_y^2\right) + 4k_5^\star u_xu_y \\
&\quad + 2\left(u_yk_6^\star + u_xk_7^\star\right) + k_8^\star + hu_x^2u_y^2.
\end{aligned}
\tag{12}
$$

Non-zero post-collision central moments $k_{0,3,4,5,6,7,8}^\star$ are

$$
\begin{aligned}
k_0^\star &= h, \\
k_3^\star &= (1-\omega)\,k_3 + \omega gh^2, \\
k_4^\star &= (1-\omega)\,k_4, \\
k_5^\star &= (1-\omega)\,k_5, \\
k_6^\star &= -hu_y\left(u_x^2 + \frac{hg}{2} - \frac{1}{3}\right), \\
k_6^\star &= -hu_x\left(u_y^2 + \frac{hg}{2} - \frac{1}{3}\right), \\
k_8^\star &= h\left[\frac{hg}{2}\left(u_x^2+u_y^2+1\right) + 3u_x^2u_y^2 - \frac{1}{3}\left(u_x^2+u_y^2\right)\right]
\end{aligned}
\tag{13}
$$

Pre-collision central moments $k_{3,4,5}$ are related to pre-collision raw-moments $r_{3,4,5}$ by

$$
\begin{aligned}
k_3 &= r_3 - h\left(u_x^2+u_y^2\right), \\
k_4 &= r_4 - h\left(u_x^2-u_y^2\right), \\
k_5 &= r_5 - hu_xu_y,
\end{aligned}
\tag{14}
$$

where

$$
\begin{aligned}
r_3 &= f_1 - f_2 + f_3 - f_4, \\
r_4 &= f_5 - f_6 + f_7 - f_8, \\
r_5 &= f_1 + f_2 + f_3 + f_4 + 2\left(f_5 + f_6 + f_7 + f_8\right).
\end{aligned}
\tag{15}
$$

Interestingly, the classical multiple-relaxation-time written in terms of raw moments can be derived as a particular case of the central-moments-based one. The interested reader can refer to Refs.[56,57] for the theoretical derivations. If RMs are considered, post-collision populations can be computed again by Eqs. (11), where post-collision raw moments now are

$$
\begin{aligned}
r_0^\star &= h, \\
r_1^\star &= hu_x, \\
r_2^\star &= hu_y, \\
r_3^\star &= (1-\omega)\,r_3 + \omega h\left(u_x^2+u_y^2+hg\right), \\
r_4^\star &= (1-\omega)\,r_4 + \omega h\left(u_x^2-u_y^2\right), \\
r_5^\star &= (1-\omega)\,r_5 + \omega hu_xu_y, \\
r_6^\star &= \frac{hu_y}{3}, \\
r_7^\star &= \frac{hu_x}{3}, \\
r_8^\star &= \frac{h}{6}\left[hg + 2\left(u_x^2+u_y^2\right)\right].
\end{aligned}
\tag{16}
$$

It is worth to note that post-collision populations in Eqs. (11) must be corrected by adding the forcing contribution (see the last term in Eq. (6)), independently from the adoption of raw or central moments.

Algorithm of computation Within the typical time step, the central-moments-based multiple-relaxation-time LBM requires the following actions.

(1) evaluate macroscopic variables by Eqs. (10);

(2) compute pre-collision raw moments by Eqs. (15);

(3) get pre-collision central moments by Eqs. (14);

(4) collide central moments by Eqs. (13);

(5) obtain post-collision raw moments by Eqs. (12);

(6) reconstruct post-collision populations by Eqs. (11);

(7) stream and advance in time by Eq. (8).

The algorithmic procedure is simpler if raw moments are adopted because it will not need the computation of central ones. In this case, the procedure moves through the following steps:

(1) evaluate macroscopic variables by Eqs. (10);

(2) compute pre-collision raw moments by Eqs. (15);

(3) collide raw moments by Eqs. (16);

(4) reconstruct post-collision populations by Eqs. (11);

(5) stream and advance in time by Eq. (8).

D. Two-stages simplified LBM in Ref.[46]

Known the solution at the time t, the simplified LBM suggests to compute the macroscopic variables at $t+1$ by a two-stages fractional step technique, *i.e.*
Predictor step:

$$\begin{aligned} h^{\dagger}\left(\boldsymbol{x}, t+1\right) &= \sum_{i} f_{i}^{eq}\left(\boldsymbol{x}-\mathbf{c}_{i}, t\right), \\ \boldsymbol{m}^{\dagger}\left(\boldsymbol{x}, t+1\right) &= \sum_{i} \mathbf{c}_{i} f_{i}^{eq}\left(\boldsymbol{x}-\mathbf{c}_{i}, t\right), \end{aligned} \tag{17}$$

and
Corrector step:

$$\begin{aligned} h\left(\boldsymbol{x}, t+1\right) &= h^{\dagger}\left(\boldsymbol{x}, t+1\right), \\ \boldsymbol{m}\left(\boldsymbol{x}, t+1\right) &= \boldsymbol{m}^{\dagger}\left(\boldsymbol{x}, t+1\right) + \\ &\quad \left(\tau-1\right) \sum_{i} \mathbf{c}_{i} f_{i}^{eq,\dagger}\left(\boldsymbol{x}+\mathbf{c}_{i}, t+1\right) - \\ &\quad \left(\tau-1\right) \boldsymbol{m}\left(\boldsymbol{x}, t\right) + \boldsymbol{F}, \end{aligned} \tag{18}$$

The relaxation time is $\tau = 1/\omega$. Note that the equilibrium state $f_i^{eq,\dagger}$ is computed by adopting the predicted values, *i.e.* $f_i^{eq,\dagger} = f_i^{eq}(h^{\dagger}, \boldsymbol{u}^{\dagger})$.

E. One-stage simplified LBM

Let us derive an SSLBM for shallow water equations building on the formulation proposed by Delgado-Gutiérrez *et al.*[47]. By applying a Taylor series expansion at the left-hand side of Eq. (6), it is possible to write the following equations:

$$\frac{f_i^{(0)} - f_i^{eq}}{\tau \Delta t} = 0, \tag{19}$$

$$\Delta f_i^{(0)} + \frac{f_i^{(1)}}{\tau \Delta t} = 0, \tag{20}$$

$$\frac{\partial f_i^{(0)}}{\partial t_1} + \left(1 - \frac{1}{2\tau}\right) \Delta f_i^{(1)} + \frac{f_i^{(2)}}{\tau \Delta t} = 0, \tag{21}$$

where $\Delta = \partial_t^{(0)} + c_{i\alpha}\partial_{\alpha}^{(0)}$ and $\Delta t = 1$ in LBM units. From Eqs. (19, 20), we obtain

$$f_i^{(0)} = f_i^{eq}, \tag{22}$$

$$f_i^{(1)} \equiv f_i^{neq} = -\tau \Delta t \Delta f_i^{eq}. \tag{23}$$

Following the SLBM, it is possible to get

$$f_i^{neq}(\boldsymbol{x}, t) = -\tau \left[f_i^{eq}(\boldsymbol{x}, t) - f_i^{eq}(\boldsymbol{x} - \mathbf{c}_i, t-1) \right]. \tag{24}$$

We can further write

$$\frac{\partial f_i^{(0)}}{\partial t_0} = -\mathbf{c}_i \cdot \boldsymbol{\nabla} f_i^{(0)} - \frac{f_i^{(1)}}{\tau \Delta t}, \tag{25}$$

$$\frac{\partial f_i^{(1)}}{\partial t_1} = -\left(1 - \frac{1}{2\tau}\right) \Delta f_i^{(1)} - \frac{f_i^{(2)}}{\tau \Delta t}. \tag{26}$$

By combining these two equations, we have

$$\frac{\partial f_i^{(0)}}{\partial t} = -\mathbf{c}_i \cdot \boldsymbol{\nabla} f_i^{(0)} - \left(1 - \frac{1}{2\tau}\right) \Delta f_i^{(1)} - \frac{f_i^{(1)} + f_i^{(2)}}{\tau \Delta t}. \tag{27}$$

Let us sum the above equation over the lattice directions, *i.e.*

$$\sum_i \left[\frac{\partial f_i^{(0)}}{\partial t} + \mathbf{c}_i \cdot \boldsymbol{\nabla} f_i^{(0)} + \left(1 - \frac{1}{2\tau}\right) \Delta f_i^{(1)} \right] = 0. \tag{28}$$

Interestingly, it is possible to write

$$\frac{\partial f_i^{(0)}}{\partial t} = f_i^{(0)}(\boldsymbol{x}, t+1) - f_i^{(0)}(\boldsymbol{x}, t), \tag{29}$$

$$\mathbf{c}_i \cdot \boldsymbol{\nabla} f_i^{(0)} = \frac{f_i^{(0)}(\boldsymbol{x} + \mathbf{c}_i, t) - f_i^{(0)}(\boldsymbol{x} - \mathbf{c}_i, t)}{2}, \tag{30}$$

$$\Delta f_i^{(1)} = \frac{\partial}{\partial t_0} f_i^{(1)} + \mathbf{c}_i \cdot \boldsymbol{\nabla} f_i^{(1)} \cong \frac{\partial f_i^{(1)}}{\partial \mathbf{c}_i} =$$

$$\frac{f_i^{(1)}(\boldsymbol{x} + \mathbf{c}_i, t) - f_i^{(1)}(\boldsymbol{x}, t)}{\partial \mathbf{c}_i} =$$

$$-\tau\left[f_i^{(0)}(\boldsymbol{x}+\mathbf{c}_i,t)-2f_i^{(0)}(\boldsymbol{x},t)+f_i^{(0)}(\boldsymbol{x}-\mathbf{c}_i,t)\right]. \tag{31}$$

Eventually, we get

$$\sum_i\Big[f_i^{(0)}(\boldsymbol{x},t+1)+2\left(\tau-1\right)f_i^{(0)}(\boldsymbol{x},t)- \left(\tau-1\right)f_i^{(0)}(\boldsymbol{x}+\mathbf{c}_i,t)- \tau f_i^{(0)}(\boldsymbol{x}-\mathbf{c}_i,t)\Big]=0. \tag{32}$$

At this point, we should note that

$$\begin{aligned}\sum_i f_i^{(0)}(\boldsymbol{x},t+1)&=h(\boldsymbol{x},t+1),\\ \sum_i f_i^{(0)}(\boldsymbol{x},t+1)\mathbf{c}_i&=\boldsymbol{m}(\boldsymbol{x},t+1),\\ \sum_i f_i^{(0)}(\boldsymbol{x},t)&=h(\boldsymbol{x},t),\\ \sum_i f_i^{(0)}(\boldsymbol{x},t)\mathbf{c}_i&=\boldsymbol{m}(\boldsymbol{x},t).\end{aligned} \tag{33}$$

By introducing the following quantities

$$\begin{aligned}h_f&=\sum_i f_i^{(0)}(\boldsymbol{x}+\mathbf{c}_i,t),\\ h_b&=\sum_i f_i^{(0)}(\boldsymbol{x}-\mathbf{c}_i,t),\\ h_c&=\sum_i f_i^{(0)}(\boldsymbol{x},t)=h(\boldsymbol{x},t),\\ \boldsymbol{m}_f&=\sum_i f_i^{(0)}(\boldsymbol{x}+\mathbf{c}_i,t)\mathbf{c}_i,\\ \boldsymbol{m}_b&=\sum_i f_i^{(0)}(\boldsymbol{x}-\mathbf{c}_i,t)\mathbf{c}_i,\\ \boldsymbol{m}_c&=\sum_i f_i^{(0)}(\boldsymbol{x},t)\mathbf{c}_i=\boldsymbol{m}(\boldsymbol{x},t),\end{aligned} \tag{34}$$

we obtain

$$\begin{aligned}h(\boldsymbol{x},t+1)&=\frac{1}{2}h_f-h_c+\frac{3}{2}h_b,\\ \boldsymbol{m}(\boldsymbol{x},t+1)&=\boldsymbol{m}_b+\left(\tau-1\right)\left(\boldsymbol{m}_f-2\boldsymbol{m}_c+\boldsymbol{m}_b\right)+\boldsymbol{F},\end{aligned} \tag{35}$$

where

$$\begin{aligned}h_f&=\sum_i f_i^{eq}(\boldsymbol{x}+\mathbf{c}_i,t),\\ h_b&=\sum_i f_i^{eq}(\boldsymbol{x}-\mathbf{c}_i,t),\\ h_c&=h(\boldsymbol{x},t),\\ \boldsymbol{m}_f&=\sum_i f_i^{eq}(\boldsymbol{x}+\mathbf{c}_i,t)\mathbf{c}_i,\\ \boldsymbol{m}_b&=\sum_i f_i^{eq}(\boldsymbol{x}-\mathbf{c}_i,t)\mathbf{c}_i,\\ \boldsymbol{m}_c&=h(\boldsymbol{x},t)\boldsymbol{u}(\boldsymbol{x},t).\end{aligned} \tag{36}$$

Eqs. (35, 36), accompanied by the expressions of the equilibrium populations in Eqs. (9), represent the core of the algorithm of the proposed SSLBM.

Before going any further, it is important to highlight two important features for the simplified LBMs. First, boundary conditions can be simply imposed by assigning the desired values of the macroscopic variables, without involving any particular treatment and additional implementation which are typical issues of population-based schemes. The interested reader can refer to Ref.[18] for a detailed explanation of the boundary conditions for populations-based LBMs. Secondly, the amount of information to be saved reduces. In fact, given M the number of points characterising a certain simulation, populations-based LBMs require to store a number of particle distribution functions equal to $2\times9\times M=18M$ per grid point. The pre-factor 2 stems from the fact that streamed populations should not overwrite post-collision (pre-streaming) ones. However, it is possible to reduce the number of information to $9M$ by adopting the swap technique[58]. Notably, other very promising approaches allowing to store only one copy of the populations have been presented by Geier & Schönherr[59] in 2017 and more recently by Lehmann[60] in 2022. In contrast to populations-based LBMs, simplified schemes require to store only the water height and the two components of the velocity vector at each lattice site at the current and previous time steps, corresponding to $2\times3\times M=6M$ values. Table I allows us to appreciate that simplified methods reduce the amount of memory of at least a factor equal to 1.5

Quantity	f_i-based	f_i-based[58]	(S)SLBM
f_i	$18M$	$9M$	0
h	0	0	$2M$
$\boldsymbol{u}$	0	0	$4M$
Total	$18M$	$9M$	$6M$

Table I. Memory required by different lattice Boltzmann schemes. Note that populations-based approaches (*i.e.*, BGK, RMs-based and CMs-based LBMs) store the same amount of information.

III. RESULTS AND DISCUSSION

In this section, we report the results of our numerical simulations. Specifically, we test the above-outlined five LBMs against five benchmark problems:

- P1: one-dimensional flow over a bump;
- P2: one-dimensional tidal wave;
- P3: one-dimensional dam break;
- P4: two-dimensional column fall;
- P5: two-dimensional circular dam break;

- P6: two-dimensional partial dam break.

When one-dimensional scenarios are considered, only 11 points are adopted in the direction y. For each run, we collect the values computed numerically in the vector $\boldsymbol{\sigma}$ and gather the corresponding reference ones in the vector $\boldsymbol{\sigma}_{\text{ref}}$. Therefore, we estimate the accuracy of the LBM by computing the L2-norm of the percentage relative error as

$$\varepsilon = \sqrt{\frac{\sum_x \left[\boldsymbol{\sigma}_{\text{ref}}(x) - \boldsymbol{\sigma}(x)\right]^2}{\sum_x \left[\boldsymbol{\sigma}_{\text{ref}}(x)\right]^2}} \times 100. \tag{37}$$

If not otherwise stated, the flow velocity is initialised equal to zero everywhere and periodic boundary conditions are adopted. When the bed is not flat, the gradient in Eq. (3) is computed by centred fourth-order-accurate finite differences. While these problems may appear simple because they neglect characteristics as surface roughness or the presence of immersed obstacles, these tests, which are very popular and well consolidated within the SWEs community, allow us to evaluate rigorously the accuracy and convergence properties of the five considered models. A summary of some relevant simulation parameters is given in Table II.

Problem	N	Δt [s]	$t_{\max}$ [s]	τ
P1	25-800	$\Delta x/20$	Until steady	0.6
P2	200-800	$\Delta x/200$	9117.5	1.0
P3	401-12801	$\Delta x/200$	4.0	0.52
P4	100	0.1	50.0	0.506
P5	200	0.01	7.2	0.56

Table II. Salient simulation parameters for each test case.

A. One-dimensional flow over a bump

In this test, a flow develops in a channel of length $L = 25\,\text{m}$ with bed topography equal to

$$z(x) = \begin{cases} 0.2\,\text{m} - 0.05\,\text{m}^{-1}\,(x - 10\,\text{m})^2 & \text{if } 8\,\text{m} < x < 12\,\text{m}, \\ 0 & \text{otherwise.} \end{cases} \tag{38}$$

Water height is initialised as

$$h(x, t = 0) = 0.5\,\text{m} - z(x). \tag{39}$$

The no-slip condition is prescribed at $x = 0$ and $x = L$. Under this setup, the flow converges to a steady state solution given by Eq. (39)[61,62]. We carry out a convergence analysis by varying the number of grid points, N, discretising the horizontal direction. Note that the corresponding grid spacing is $\Delta x = L/N\,\text{m}$ and the time step is $\Delta t = \Delta x/\left(20\,\text{m}\,\text{s}^{-1}\right)$. The relaxation time is set to $\tau = 0.6$. The L2-norms of the relative error between our numerical predictions and the analytical solution are reported in Table III and their logarithms are sketched in Figure 1. The SSLBM shows the poorest accuracy and the lowest convergence rate (*i.e.*, the slopes of the lines), that is equal to 1.5. The other methods exhibit errors which are substantially overlapped, with an optimal convergence rate equal to 2.

N	BGK	RMs	CMs	SLBM	SSLBM
25	1.2340	1.2340	1.2447	1.1430	1.5806
50	0.3094	0.3094	0.3106	0.2853	0.5510
100	0.0773	0.0773	0.0776	0.0713	0.1938
200	0.0193	0.0193	0.0194	0.0178	0.0688
400	0.0048	0.0048	0.0048	0.0045	0.0244
800	0.0012	0.0012	0.0012	0.0011	0.0086

Table III. One-dimensional flow over a bump: L2-norm of the percentage relative error of different LBMs with respect to the analytical predictions.

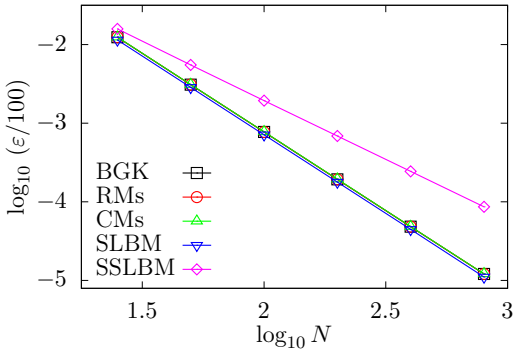

Figure 1. One-dimensional flow over a bump: convergence analysis.

Such findings are surprising because the SSLBM is expected to keep the second order of accuracy of the lattice Boltzmann formulation. This pushes as to further dive into this aspect. By fixing $N = 400$, we repeat our simulations by varying the relaxation time. While populations-based schemes and the SLBM do no show any dependence of the solution on τ, the SSLBM is strongly affected by the chosen value of the relaxation time. In fact, Figure 2 depicts the values of ε obtained by the SSLBM runs as a function of τ, with the error being minimised at $\tau = 0.75$. Let us repeat the convergence analysis by varying N and fixing $\tau = 0.75$. Table IV reports the values of ε against N. It is possible to appreciate that the SSLBM is second-order accurate, with errors slightly smaller than those obtained by the other LBMs.

B. One-dimensional tidal wave

The rise of a tidal wave is a very popular case to test the accuracy of any numerical method to solve SWEs[63].

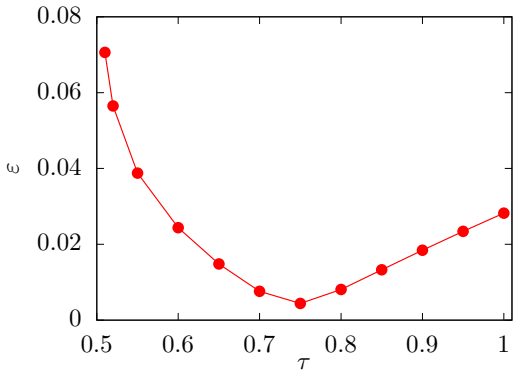

Figure 2. One-dimensional flow over a bump: L2-norm of the percentage relative error of the SSLBM for different values of the relaxation time. The number of points discretising the horizontal direction is $N = 400$.

N	25	50	100	200	400	800
$\tau = 0.75$	1.1293	0.2819	0.0704	0.0176	0.0044	0.0011

Table IV. One-dimensional flow over a bump: L2-norm of the percentage relative error of the SSLBM for different values of N. The relaxation time is $\tau = 0.75$.

Let us consider a channel of length $L = 14\,\mathrm{km}$. The bed surface is $z(x) = H(x = 0) - H(x)$, where

$$H(x) = 50.5 - \frac{40x}{L} - 10\,\sin\left[\pi\left(\frac{4x}{L} - \frac{1}{2}\right)\right]. \quad (40)$$

At $t = 0$, the water height is set equal to $H(x)$. The problem admits analytical solution in the form

$$h_{\mathrm{an}}(x,t) = H(x) + 4 - 4\,\sin\left[\pi\left(\frac{4t}{86400} + \frac{1}{2}\right)\right]. \quad (41)$$

Boundary conditions consist of imposing $h(x = 0, t) = h_{\mathrm{an}}(x = 0, t)$ and $\boldsymbol{u}(x = L, t) = 0$. We carry out several numerical runs by changing the number of grid points discretising the horizontal direction as $N = 200, 400, 600, 800$. Note that the corresponding grid spacing is $\Delta x = L/(N-1)\,\mathrm{m}$ and the time step is $\Delta t = \Delta x/\left(200\,\mathrm{m\,s^{-1}}\right)$. In this test, we set $\tau = 1$ and simulations last until $t = 9117.5\,\mathrm{s}$. Making reference at Figure 3 and Table V, populations-based approaches are considerably more accurate than the simplified scheme. Notably, the one-stage model enhances the accuracy of the numerical solution by the $\sim 10\%$ with respect to the two-stages counterpart, thus corroborating the behaviour experienced in Ref.[48] The BGK LBM, in turn, exhibits an error that is one order of magnitude lower. Results obtained by the adoption of RMs and CMs are not reported because they overlap values obtained by BGK runs.

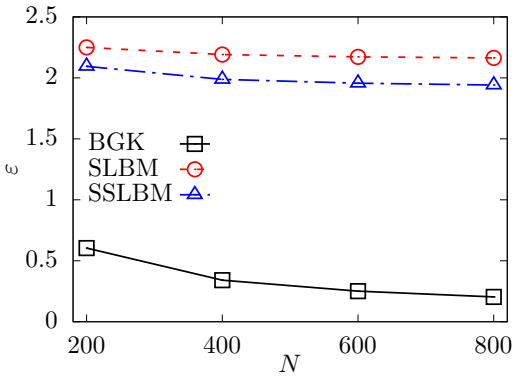

Figure 3. One-dimensional tidal wave: L2-norm of the percentage relative error for different values of N. Findings are obtained by BGK LBM (black solid line with squares), SLBM (red dashed line with circles) and SSLBM (blue dash-dotted line with triangles). Values computed by populations-based schemes are overlapped, hence only those obtained by BGK runs are plotted.

N	BGK	SLBM	SSLBM
200	0.6043	2.2501	2.0944
400	0.3408	2.1910	1.9873
600	0.2505	2.1726	1.9561
800	0.2040	2.1637	1.9413

Table V. One-dimensional tidal wave: L2-norm of the percentage relative error of different LBMs with respect to the analytical predictions.

C. One-dimensional dam break

A very famous test is represented by the one-dimensional dam break. Let us consider a flat channel of length $L = 100\,\mathrm{m}$ where the water height is initialised as

$$h(x) = \begin{cases} h_l & \text{if } x < x_D, \\ h_r & \text{otherwise}, \end{cases} \quad (42)$$

where $h_l = 10\,\mathrm{m}$ and $h_r = 5\,\mathrm{m}$. Due to the presence of the discontinuity located at $x_D = 50\,\mathrm{m}$, two waves are generated: a leftward refraction one and a rightward shock one. The problem admits analytical solution in the form[64]

$$h_{\mathrm{an}}(x,t) = \begin{cases} h_l & \text{if } x \le x_A, \\ \frac{4}{g}\left(\sqrt{gh_l} - \frac{x - x_D}{2t}\right)^2 & \text{if } x_A(t) < x \le x_B(t), \\ \frac{c_m^2}{g} & \text{if } x_B(t) < x \le x_C(t), \\ h_r & \text{otherwise}, \end{cases} \quad (43)$$

where

$$x_A(t) = x_D - t\sqrt{gh_l},$$
$$x_B(t) = x_D + t\left(2\sqrt{gh_l} - 3c_m\right),$$
$$x_C(t) = x_D + t\frac{2c_m^2\left(\sqrt{gh_l} - c_m\right)}{c_m^2 - gh_r}, \tag{44}$$

with c_m being the solution of the equation

$$-8gh_r c_m^2\left(\sqrt{gh_l} - c_m\right)^2 + \left(c_m^2 - gh_r\right)^2\left(c_m^2 + gh_r\right) = 0 \tag{45}$$

which corresponds to a water height of

$$h_m = \frac{c_m^2}{g}, \tag{46}$$

with $h_l < h_m < h_r$. In our runs, we set $\tau = 0.52$ and $\Delta t = L/(200N)$. Simulations last until $t = 4\,\mathrm{s}$. In Figure 4, the profiles of the water height obtained by BGK, SLBM and SSLBM analyses are sketched. Specifically, we adopt three different grid resolutions, *i.e.* $N =$ 101, 401, 12801. We do not depict findings achieved by RMs-based and CMs-based collision operators because these are overlapped to the BGK ones. From Figure 4, we can appreciate that the approaches generate numerical solutions which are progressively closer to the analytical predictions as N grows. However, the zoomed views provide more interesting insights. It is possible to observe that the solution given by the SLBM exhibits the largest deviations from the analytical solution. The adoption of the SSLBM alleviates this behaviour and generates results which are very similar to those obtained by populations-based schemes. A quantitative summary of the discrepancies between analytical predictions and the numerical solution is provided in Table VI, where the percentage relative errors are reported. This table confirms the low performance of the SLBM.

N	BGK	SLBM	SSLBM
401	1.1717	1.3835	1.1902
801	0.7885	0.9413	0.8323
12801	0.1895	0.3621	0.2234

Table VI. One-dimensional dam break: L2-norm of the percentage relative error of different LBMs with respect to the analytical predictions.

D. Two-dimensional column fall

The fourth test deals with the case devised in Ref.[65]. Let us consider a square domain of size $L \times L$, with $L = 4000\,\mathrm{m}$. The initial conditions are

$$h(\boldsymbol{x}, t=0) = 10\,\mathrm{m} \quad \text{if } (x-x_c)^2 + (y-y_c)^2 \leq R^2,$$
$$h(\boldsymbol{x}, t=0) = 5\,\mathrm{m} \quad \text{otherwise}, \tag{47}$$

where $R = 800\,\mathrm{m}$ and $x_c = y_c = L/2$. In our simulations, we adopt 100 points in each direction, the time step is equal to $\Delta t = 0.1\,\mathrm{s}$ and the relaxation time is $\tau = 0.506$[21]. In Figure 5, the profiles of the water height at $t = 50\,\mathrm{s}$ are plotted for different LBMs, together with results obtained by another effort carried out within the LBM community[21]. Populations-based LBMs show again results which are well overlapped, hence we plot only the outcome of the BGK run. BGK and SSLBM generate very similar results. The SLBM offers the smoothest solution and we link this behaviour to its higher dissipation properties[48,49]. The mismatch between our findings and those reported in Ref.[21] could be explained by the fact that the latter adopted multi-block grid refinements, which are expected to increase the stability and accuracy of the algorithm, together with providing us with a smoother profile of the water height.

Eventually, we sketch the water height field at salient time instants in Figure 6. From these plots, it is possible to confirm that the SLBM is the most dissipative method. In fact, the sharp knees in the interface experienced by the BGK run (especially during the earliest stages of the simulation) here appears drastically damped. This is partially alleviated by the SSLBM, whose water height field is closer to the one generated by the BGK LBM.

E. Two-dimensional partial dam break

We conclude our numerical campaign by investigating the flow physics generated by a partial dam break[66]. Let us consider a square domain enclosed by no-slip walls, where each side has length $L = 200\,\mathrm{m}$. The water height is initialised as in Eqs. (42). The two regions with different water heights are separated by a y-aligned wall with a breach. The width of the wall is equal to 10 m and its centre is located at $x = L/2$. The wall breach extends from $y = 95\,\mathrm{m}$ to $y = 170\,\mathrm{m}$. 200 points are adopted to discretised each side of the domain, the time step is equal to 0.01 s and the relaxation time is set to $\tau = 0.6$. Figure 7 depicts the profile of the water height along an x-aligned line passing through the middle of the breach. One can immediately appreciate that there is a strong agreement between the solution provided by all the considered schemes. The evolution of the water height at representative time instants is plotted in Figure 8. Here, it is possible to observe a leftward refraction wave and a shock rightward one propagating from the breach into the fluid domain. This corroborates the behaviour of the fluid flow experienced in Ref.[21,66].

IV. CONCLUSIONS

In this work, we evaluated the performance of five lattice Boltzmann methods to simulate shallow water flows. Schemes can be split into two groups. The former is composed of three approaches (*i.e.*, BGK, RMs-based

Accepted to Phys. Fluids 10.1063/5.0147175

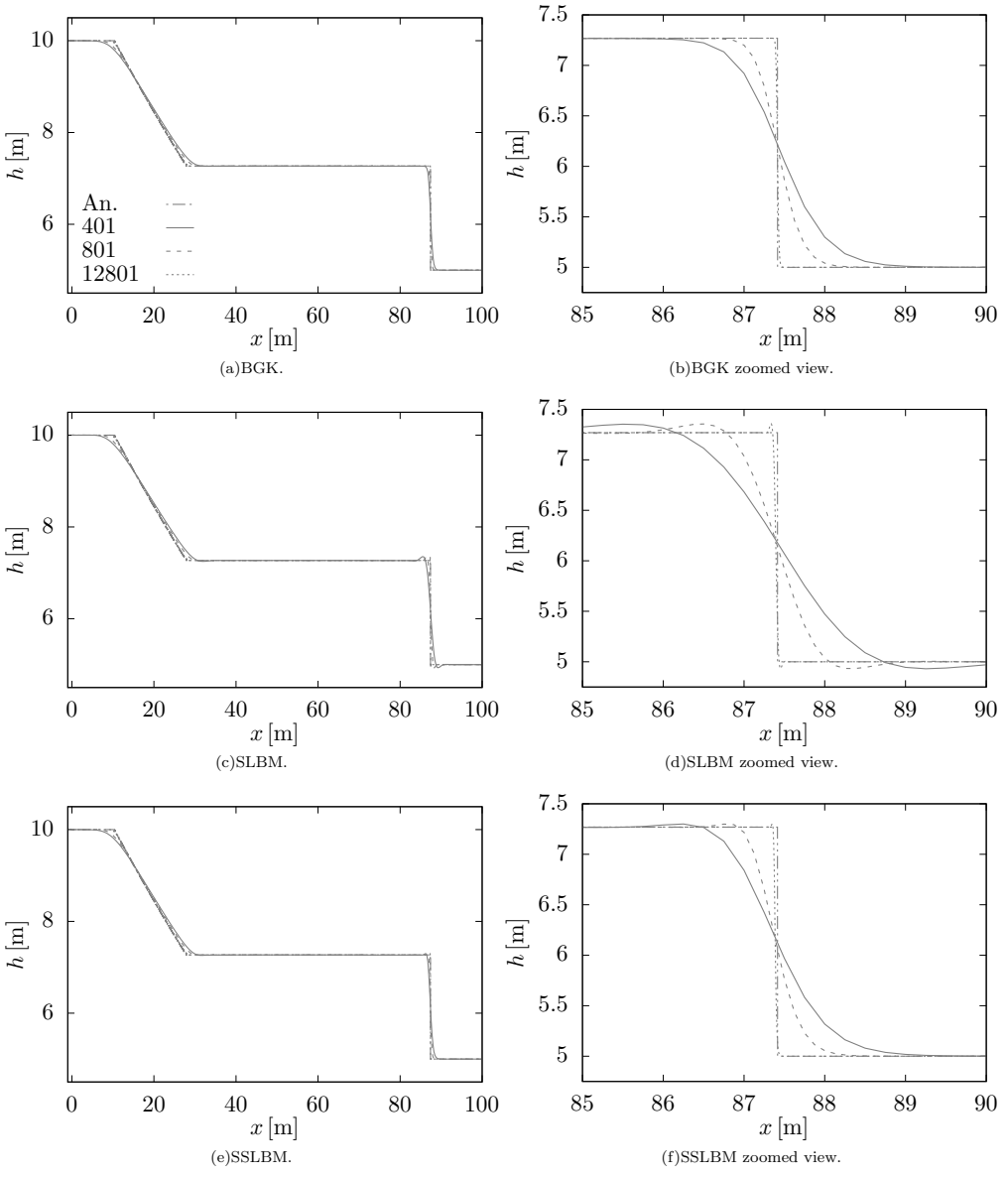

(a)BGK. (b)BGK zoomed view.

(c)SLBM. (d)SLBM zoomed view.

(e)SSLBM. (f)SSLBM zoomed view.

Figure 4. One-dimensional dam break: water height obtained by different LBMs at $t = 4\,\mathrm{s}$. Right panels sketch the zoomed views of the sharpest region of the domain. Results are obtained by computing the analytical solution on 12801 points (dash-double-dotted line), and through our numerical analyses by varying the number of points discretising as $N = 401$ (continuous line), 801 (dashed line) and 12801 (dotted line).

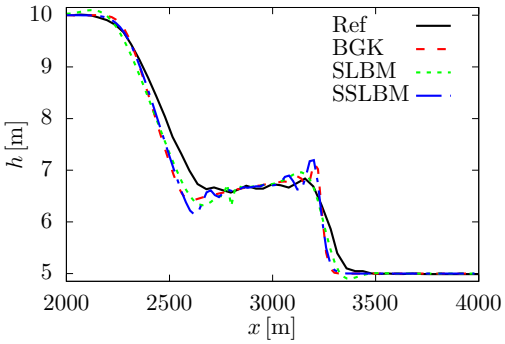

Figure 5. Two-dimensional column fall: water height at $t = 50\,\mathrm{s}$ obtained by different LBMs and results obtained in Ref.[21] (Ref).

and CMs-based LBMs), which involve the computation of particle distribution functions. The latter comprises the SLBM and SSLBM, which need to store only macroscopic variables. Overall, populations-based approaches are more accurate. However, their adoption leads inevitably to higher memory consumption and to perform additional implementation for boundary treatment. The SLBM suffers from high numerical dissipation, that is partially alleviated by the SSLBM. This, in turn, appears very sensitive to the choice of the relaxation time.

CONFLICT OF INTEREST

The authors have no conflict of interest to disclose.

DATA AVAILABILITY STATEMENT

The data that support the findings of this study are available from the corresponding author upon reasonable request.

ACKNOWLEDGMENTS

The author would like to thank the four anonymous referees, who helped to improve the quality of the manuscript with their very useful comments.

Accepted to Phys. Fluids 10.1063/5.0147175

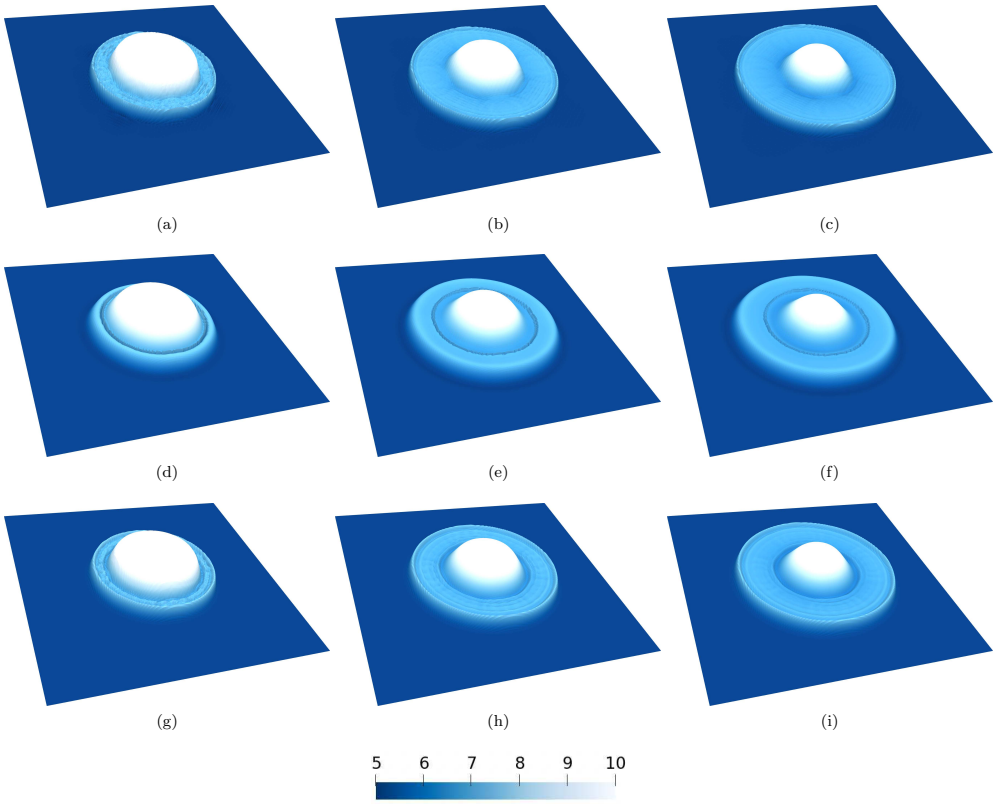

Figure 6. Two-dimensional column fall: water height field by BGK (a, b, c), SLBM (d, e, f) and SSLBM (g, h, i) at $t = 20\,\mathrm{s}$ (a, d, g), 40 s (b, e, h) and 50 s (c, f, i).

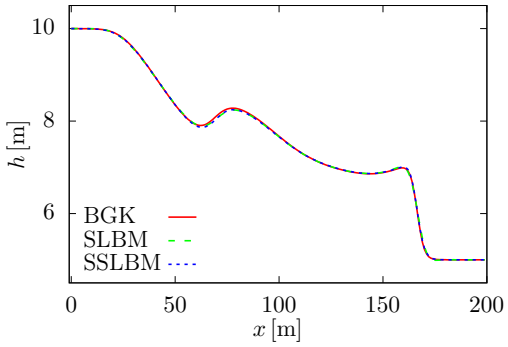

Figure 7. Two-dimensional partial dam break: water height at $t = 7.2\,\mathrm{s}$ obtained by different LBMs.

Accepted to Phys. Fluids 10.1063/5.0147175

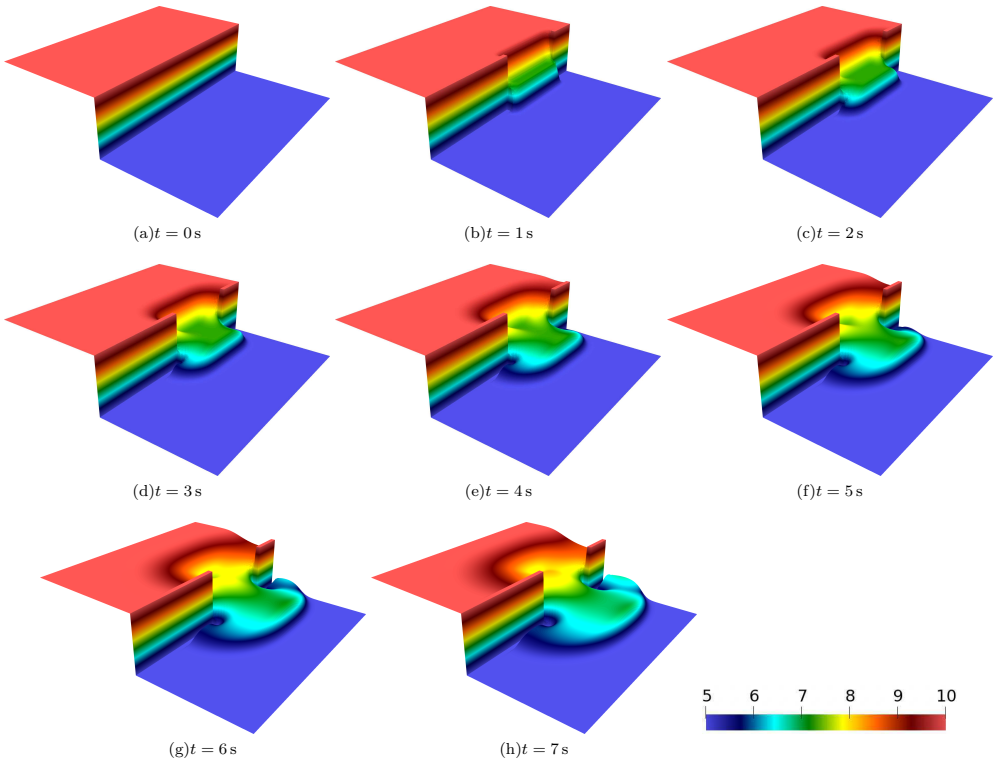

Figure 8. Two-dimensional partial dam break: water height field obtained by the SSLBM at representative time instants.

REFERENCES

[1]C. B. Vreugdenhil, *Numerical methods for shallow-water flow*, Vol. 13 (Springer Science & Business Media, 1994).
[2]J. R. Holton, "An introduction to dynamic meteorology," American Journal of Physics **41**, 752–754 (1973).
[3]R. L. Higdon, "Numerical modelling of ocean circulation," Acta Num **15**, 385–470 (2006).
[4]I. Özgen, J. Zhao, D. Liang, and R. Hinkelmann, "Urban flood modeling using shallow water equations with depth-dependent anisotropic porosity," J Hydrol **541**, 1165–1184 (2016).
[5]K. Hu, C. Mingham, and D. Causon, "Numerical simulation of wave overtopping of coastal structures using the non-linear shallow water equations," Coast Eng **41**, 433–465 (2000).
[6]Y.-S. Cho, D.-H. Sohn, and S. O. Lee, "Practical modified scheme of linear shallow-water equations for distant propagation of tsunamis," Ocean Eng **34**, 1769–1777 (2007).
[7]A. Decoene, L. Bonaventura, E. Miglio, and F. Saleri, "Asymptotic derivation of the section-averaged shallow water equations for natural river hydraulics," Math Mod Meth Appl S **19**, 387–417 (2009).
[8]V. Casulli, "Semi-implicit finite difference methods for the two-dimensional shallow water equations," J Comput Phys **86**, 56–74 (1990).
[9]E. F. Toro, "Riemann problems and the waf method for solving the two-dimensional shallow water equations," Philos T R Soc A **338**, 43–68 (1992).
[10]J. G. Zhou, "Velocity-depth coupling in shallow-water flows," J Hydraul Eng **121**, 717–724 (1995).
[11]F. Alcrudo and P. Garcia-Navarro, "A high-resolution godunov-type scheme in finite volumes for the 2d shallow-water equations," Int J Numer Meth Fl **16**, 489–505 (1993).
[12]T. Krüger, H. Kusumaatmaja, A. Kuzmin, O. Shardt, G. Silva, and E. M. Viggen, *The Lattice Boltzmann Method: Principles and Practice* (Springer, 2016).
[13]S. Succi, *The Lattice Boltzmann Equation: For Complex States of Flowing Matter* (Oxford University Press, 2018).
[14]C. K. Aidun and J. R. Clausen, "Lattice-boltzmann method for complex flows," Ann. Rev. Fluid Mech **42**, 439–472 (2010).
[15]H. Chen, S. Chen, and W. Matthaeus, "Recovery of the Navier-Stokes equations using a lattice-gas Boltzmann method," Phys. Rev. Lett. **45**, R5339–R5342 (1992).
[16]D. Dapelo, S. Simonis, M. J. Krause, and J. Bridgeman, "Lattice-boltzmann coupled models for advection–diffusion flow on a wide range of péclet numbers," J Comput Sci **51**, 101363 (2021).
[17]A. De Rosis, "Modeling epidemics by the lattice Boltzmann method," Phys. Rev. E **102**, 023301 (2020).
[18]J. Zhou, "A lattice boltzmann model for the shallow water equations," Comput. Method Appl. M. **191**, 3527–3539 (2002).
[19]J. Zhou, "A lattice boltzmann model for the shallow water equations with turbulence modeling," Int. J. Mod. Phys. C **13**, 1135–1150 (2002).
[20]J. G. Zhou, *Lattice Boltzmann methods for shallow water flows*, Vol. 4 (Springer, 2004).
[21]H. Liu, J. G. Zhou, and R. Burrows, "Lattice boltzmann simulations of the transient shallow water flows," Adv Water Resour **33**, 387–396 (2010).
[22]K. R. Tubbs and F. T.-C. Tsai, "Multilayer shallow water flow using lattice boltzmann method with high performance computing," Adv. Water Resour. **32**, 1767–1776 (2009).
[23]M. L. Rocca, C. Adduce, V. Lombardi, G. Sciortino, and R. Hinkelmann, "Development of a lattice boltzmann method for two-layered shallow-water flow," Int. J. Num. Meth. Fl. **70**, 1048–1072 (2012).
[24]P. Prestininzi, G. Sciortino, and M. L. Rocca, "On the effect of the intrinsic viscosity in a two-layer shallow water lattice boltzmann model of axisymmetric density currents," J. Hydraul. Res. **51**, 668–680 (2013).
[25]P. Prestininzi, A. Montessori, M. La Rocca, and G. Sciortino, "Simulation of arrested salt wedges with a multi-layer shallow water lattice boltzmann model," Adv. Water Resour. **96**, 282–289 (2016).
[26]J. Latt and B. Chopard, "Lattice boltzmann method with regularized pre-collision distribution functions," Math. Comput. Simulat. **72**, 165 – 168 (2006).
[27]P. J. Dellar, "Nonhydrodynamic modes and a priori construction of shallow water lattice boltzmann equations," Phys. Rev. E **65**, 036309 (2002).
[28]D. d'Humières, "Multiple-relaxation-time lattice Boltzmann models in three dimensions," Philos. T. R. Soc. A **360**, 437–451 (2002).
[29]S. Marié, D. Ricot, and P. Sagaut, "Comparison between lattice boltzmann method and navier–stokes high order schemes for computational aeroacoustics," J. Comput. Phys. **228**, 1056–1070 (2009).
[30]K. R. Tubbs and F. T.-C. Tsai, "Gpu accelerated lattice boltzmann model for shallow water flow and mass transport," Int. J. Num. Meth. Fl. **86**, 316–334 (2011).
[31]Y. Peng, J. Zhang, and J. Zhou, "Lattice boltzmann model using two relaxation times for shallow-water equations," J Hydraul Eng **142**, 06015017 (2015).
[32]X. B. Nie, X. Shan, and H. Chen, "Galilean invariance of lattice boltzmann models," Europhys. Lett. **81**, 34005 (2008).
[33]M. Geier, A. Greiner, and J. Korvink, "Cascaded digital lattice Boltzmann automata for high Reynolds number flow," Phys. Rev. E **73**, 066705 (2006).
[34]A. De Rosis and K. H. Luo, "Role of higher-order hermite polynomials in the central-moments-based lattice boltzmann framework," Phys. Rev. E **99**, 013301 (2019).
[35]M. Geier, A. Greiner, and J. Korvink, "Properties of the cascaded lattice Boltzmann automaton," Int. J. Mod. Phys. C **18**, 455–462 (2007).
[36]M. Geier, A. Greiner, and J. Korvink, "A factorized central moment lattice Boltzmann method," Eur. Phys. J-Spec. Top. **171**, 55–61 (2009).
[37]S. Geller, S. Uphoff, and M. Krafczyk, "Turbulent jet computations based on MRT and Cascaded Lattice Boltzmann models," Comput. Math. Appl. **65**, 1956–1966 (2013).
[38]Y. Ning, K. N. Premnath, and D. V. Patil, "Numerical study of the properties of the central moment lattice boltzmann method," Int. J. Numer. Meth. Fl. **82**, 59–90 (2016).
[39]Z. Chen, C. Shu, Y. Wang, L. Yang, and D. Tan, "A simplified lattice boltzmann method without evolution of distribution function," Adv Appl Math Mech **9**, 1–22 (2017).
[40]Z. Chen, C. Shu, and D. Tan, "Immersed boundary-simplified lattice boltzmann method for incompressible viscous flows," Phys Fluids **30**, 053601 (2018).
[41]Z. Chen, C. Shu, D. Tan, and C. Wu, "On improvements of simplified and highly stable lattice boltzmann method: Formulations, boundary treatment, and stability analysis," Int J Numer Meth Fl **87**, 161–179 (2018).
[42]Z. Chen, C. Shu, and D. Tan, "High-order simplified thermal lattice boltzmann method for incompressible thermal flows," Int J Heat Mass Tran **127**, 1–16 (2018).
[43]Z. Chen, C. Shu, and D. S. Tan, "The simplified lattice boltzmann method on non-uniform meshes," Commun. Comput. Phys **23**, 1131 (2018).
[44]Z. Chen and C. Shu, "On numerical diffusion of simplified lattice boltzmann method," Int J Numer Meth Fl **92**, 1198–1211 (2020).
[45]Z. Chen, C. Shu, L. Yang, X. Zhao, and N. Liu, "Immersed boundary-simplified thermal lattice boltzmann method for incompressible thermal flows," Phys Fluids **32**, 013605 (2020).
[46]N. Maquignon, H. Smaoui, P. Sergent, and B. Bader, "A simplified and stable lattice boltzmann shallow water model," J Phys Conf Ser **2202**, 012055 (2022).
[47]A. Delgado-Gutiérrez, P. Marzocca, D. Cárdenas, and O. Probst, "A single-step and simplified graphics processing unit lattice boltzmann method for high turbulent flows," Int J Numer Meth

Fl **93**, 2339–2361.
[48]A. De Rosis, R. Liu, and A. Revell, "One-stage simplified lattice boltzmann method for two- and three-dimensional magnetohydrodynamic flows," Phys Fluids **33**, 085114 (2021).
[49]L. Vienne and E. Lévêque, "Recursive finite-difference lattice boltzmann schemes," Comput Math Appl **96**, 95–108 (2021).
[50]A. De Rosis, "A central moments-based lattice boltzmann scheme for shallow water equations," Comput. Method. Appl. M. **319**, 379–392 (2017).
[51]J. Meng, X.-J. Gu, D. R. Emerson, Y. Peng, and J. Zhang, "Discrete boltzmann model of shallow water equations with polynomial equilibria," Int J Mod Phys C **29**, 1850080 (2018).
[52]M. La Rocca, A. Montessori, P. Prestininzi, and S. Succi, "A multispeed discrete boltzmann model for transcritical 2d shallow water flows," J. Comput. Phys. **284**, 117–132 (2015).
[53]A. De Rosis, "Non-orthogonal central moments relaxing to a discrete equilibrium: A d2q9 lattice boltzmann model," Europhys. Lett. **116**, 44003 (2017).
[54]A. De Rosis, "Nonorthogonal central-moments-based lattice boltzmann scheme in three dimensions," Phys. Rev. E **95**, 013310 (2017).
[55]A. De Rosis and A. Tafuni, "A phase-field lattice boltzmann method for the solution of water-entry and water-exit problems," Comput-Aided Civ Inf **37**, 832–847 (2022).
[56]A. De Rosis, R. Huang, and C. Coreixas, "Universal formulation of central-moments-based lattice Boltzmann method with external forcing for the simulation of multiphysics phenomena," Phys. Fluids **31**, 117102 (2019).
[57]A. De Rosis and C. Coreixas, "Multiphysics flow simulations using d3q19 lattice boltzmann methods based on central moments," Phys Fluids **32**, 117101 (2020).
[58]J. Latt, "Technical report: How to implement your ddqq dynamics with only q variables per node (instead of 2q)," Tufts University , 1–8 (2007).
[59]M. Geier and M. Schönherr, "Esoteric twist: An efficient in-place streaming algorithmus for the lattice boltzmann method on massively parallel hardware," Computation **5** (2017), 10.3390/computation5020019.
[60]M. Lehmann, "Esoteric pull and esoteric push: Two simple in-place streaming schemes for the lattice boltzmann method on gpus," Computation **10** (2022), 10.3390/computation10060092.
[61]O. Delestre, C. Lucas, P.-A. Ksinant, F. Darboux, C. Laguerre, T.-N. Vo, F. James, S. Cordier, *et al.*, "Swashes: a compilation of shallow water analytic solutions for hydraulic and environmental studies," Int. J. Num. Meth. Fl. **72**, 269–300 (2013).
[62]S. Li, P. Huang, and J. Li, "A modified lattice boltzmann model for shallow water flows over complex topography," Int J Numer Meth Fl **77**, 441–458 (2015).
[63]A. Bermudez and M. E. Vazquez, "Upwind methods for hyperbolic conservation laws with source terms," Comput Fluids **23**, 1049–1071 (1994).
[64]J. J. Stoker, *Water waves: The mathematical theory with applications*, Vol. 36 (John Wiley & Sons, 1992).
[65]J. Murillo, P. García-Navarro, J. Burguete, and P. Brufau, "A conservative 2d model of inundation flow with solute transport over dry bed," Int. J. Num. Meth. Fl. **52**, 1059–1092 (2006).
[66]R. J. Fennema and M. H. Chaudhry, "Explicit methods for 2-d transient free surface flows," J Hydraul Eng **116**, 1013–1034 (1990).

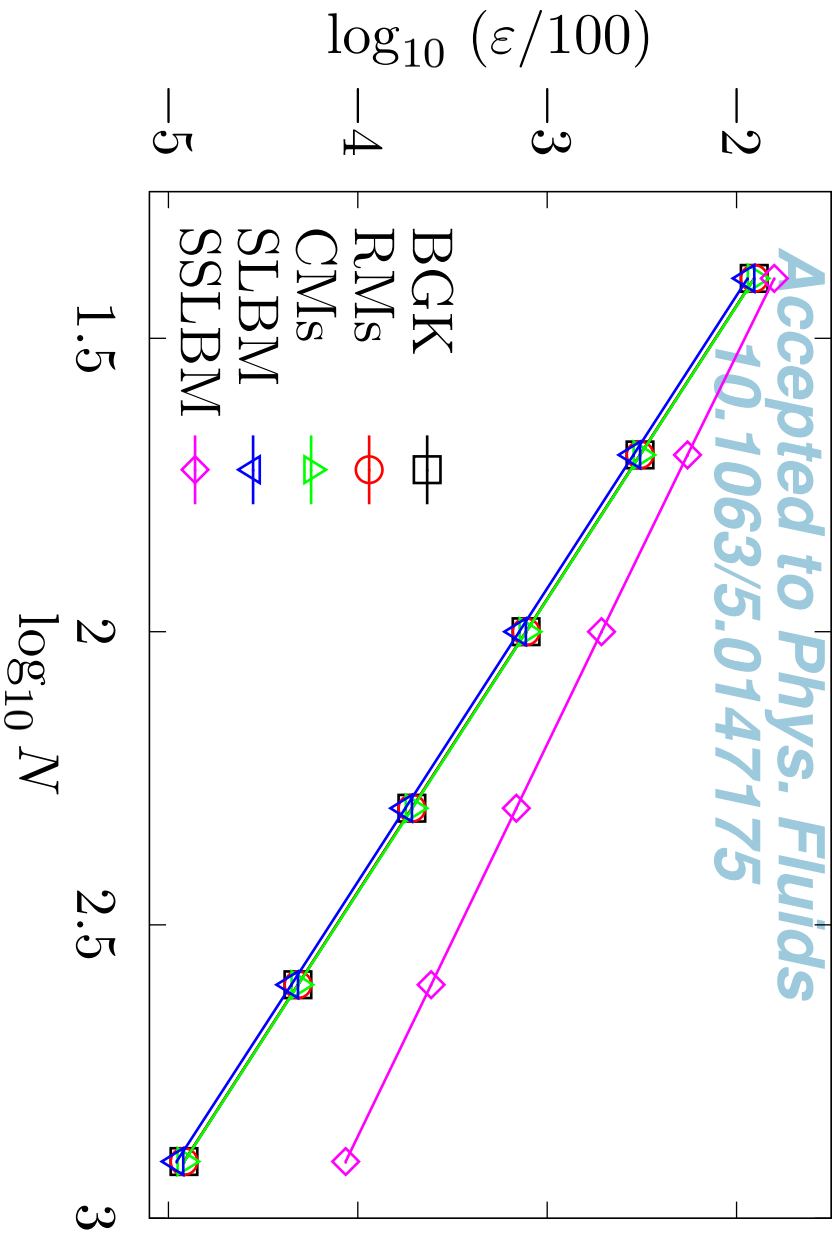

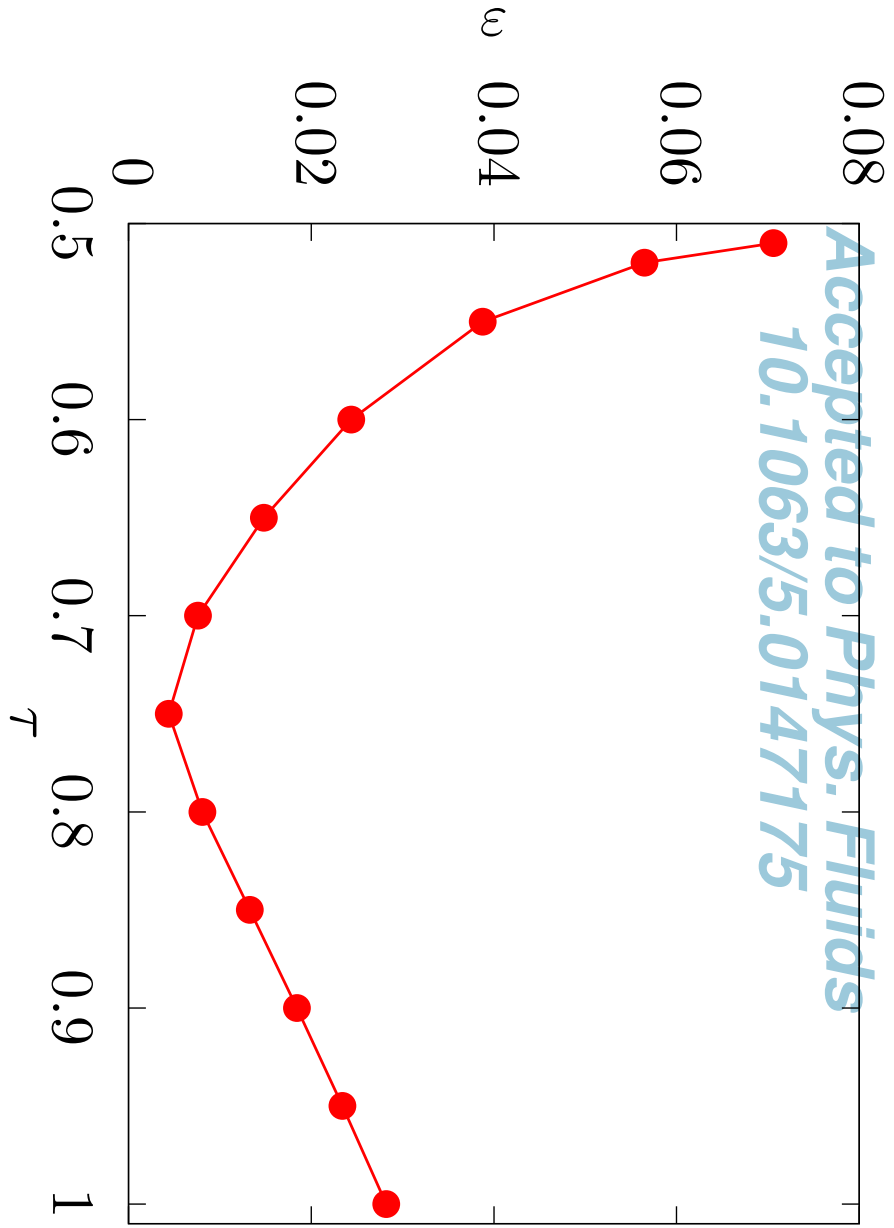

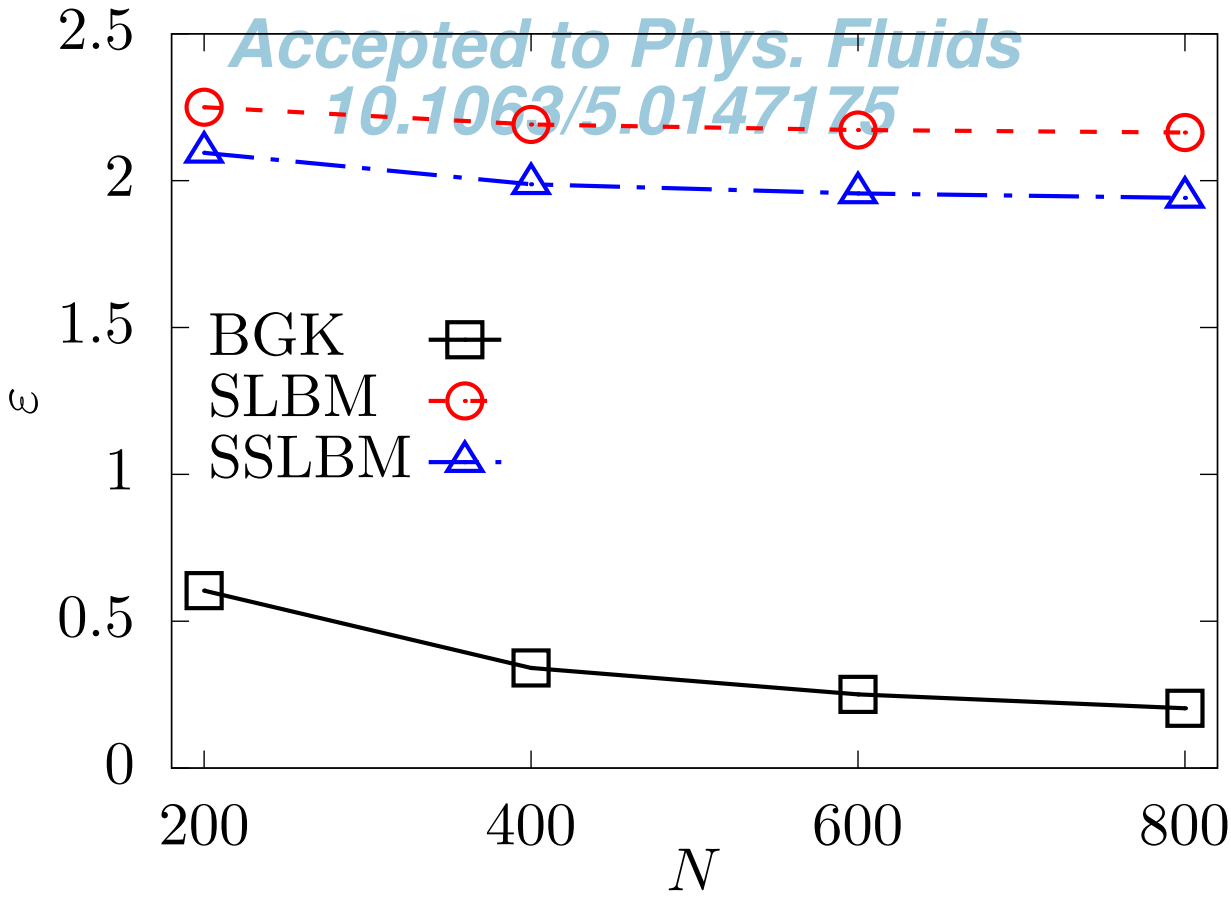

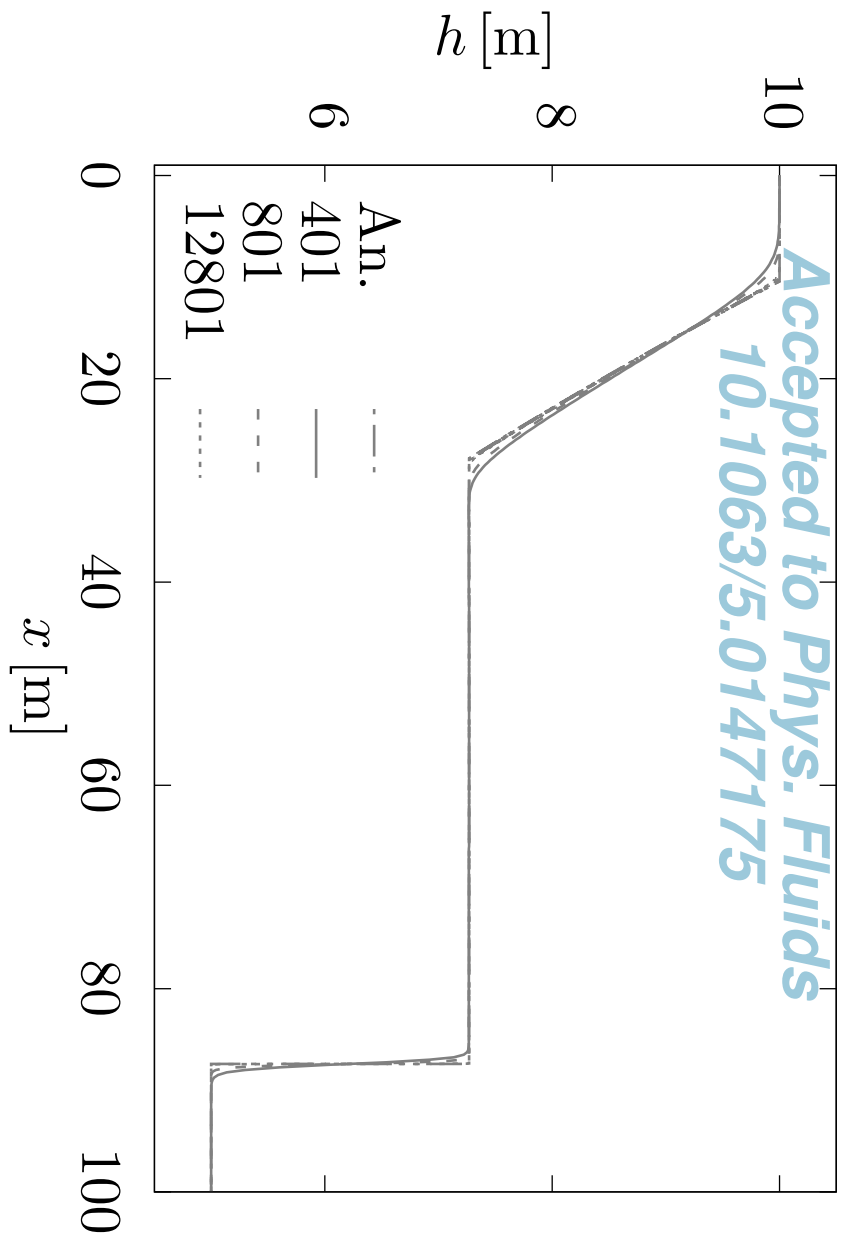

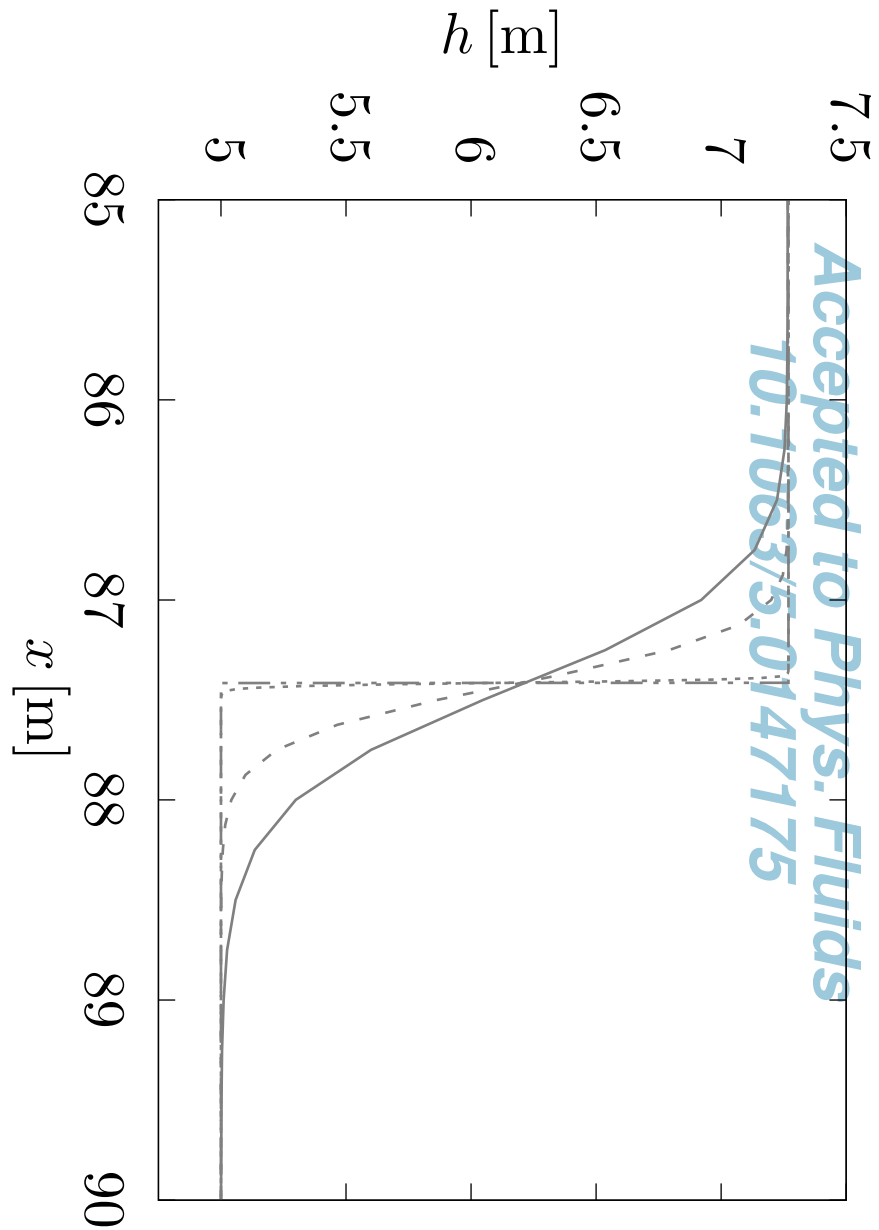

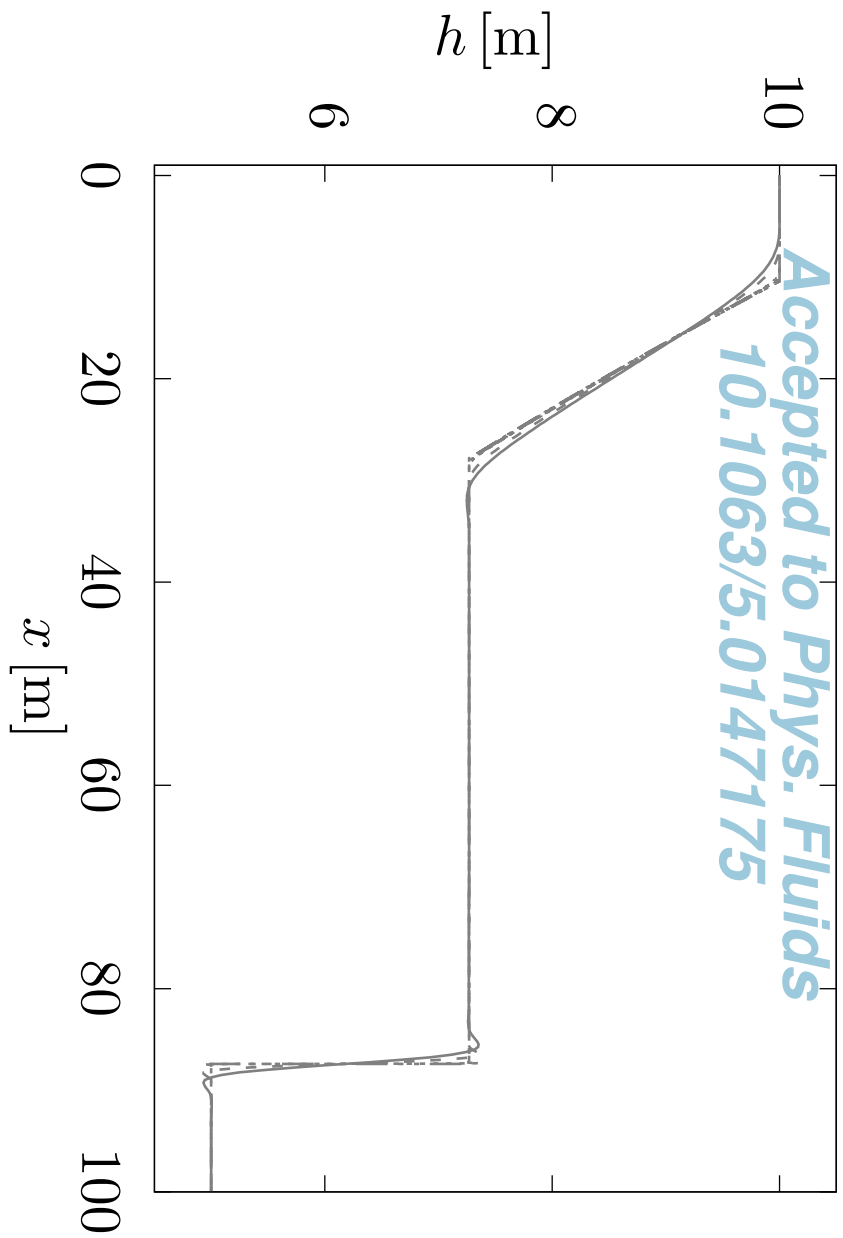

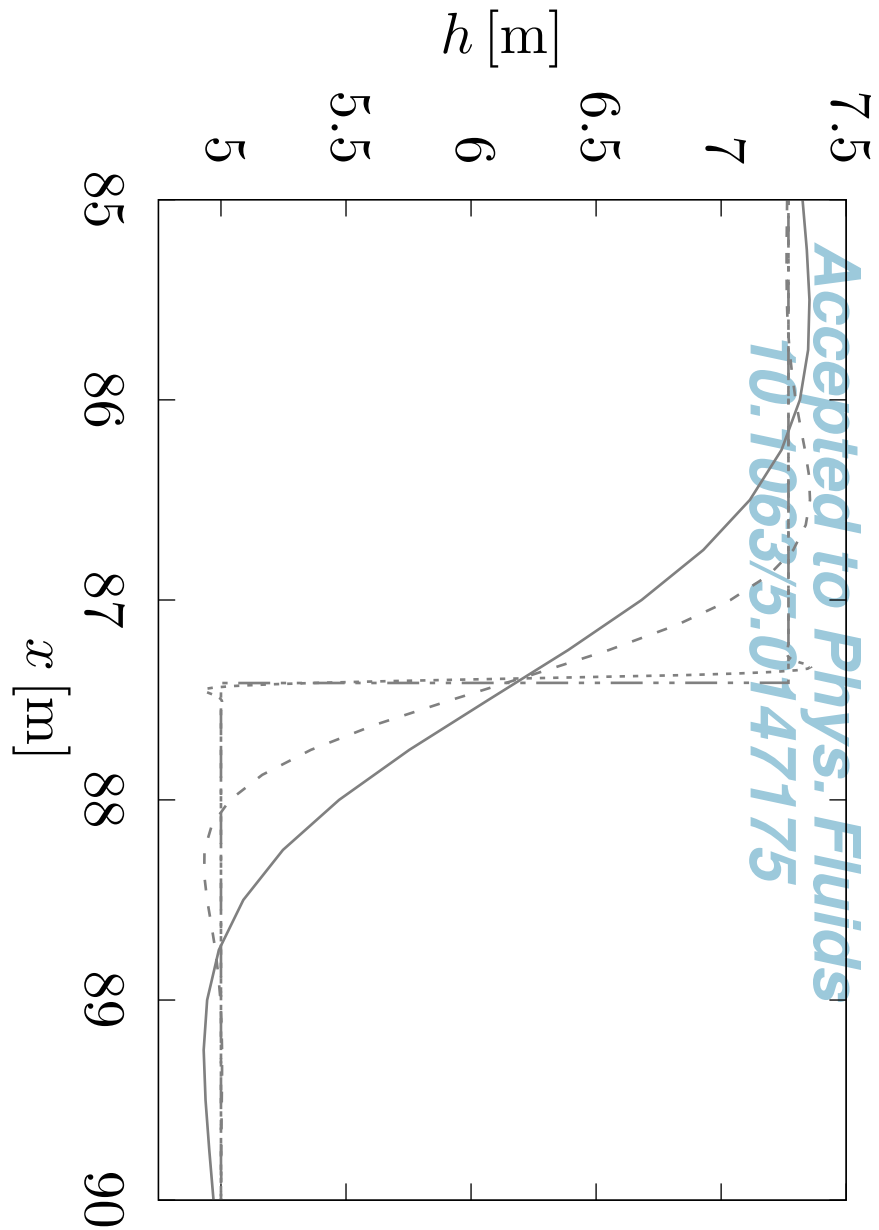

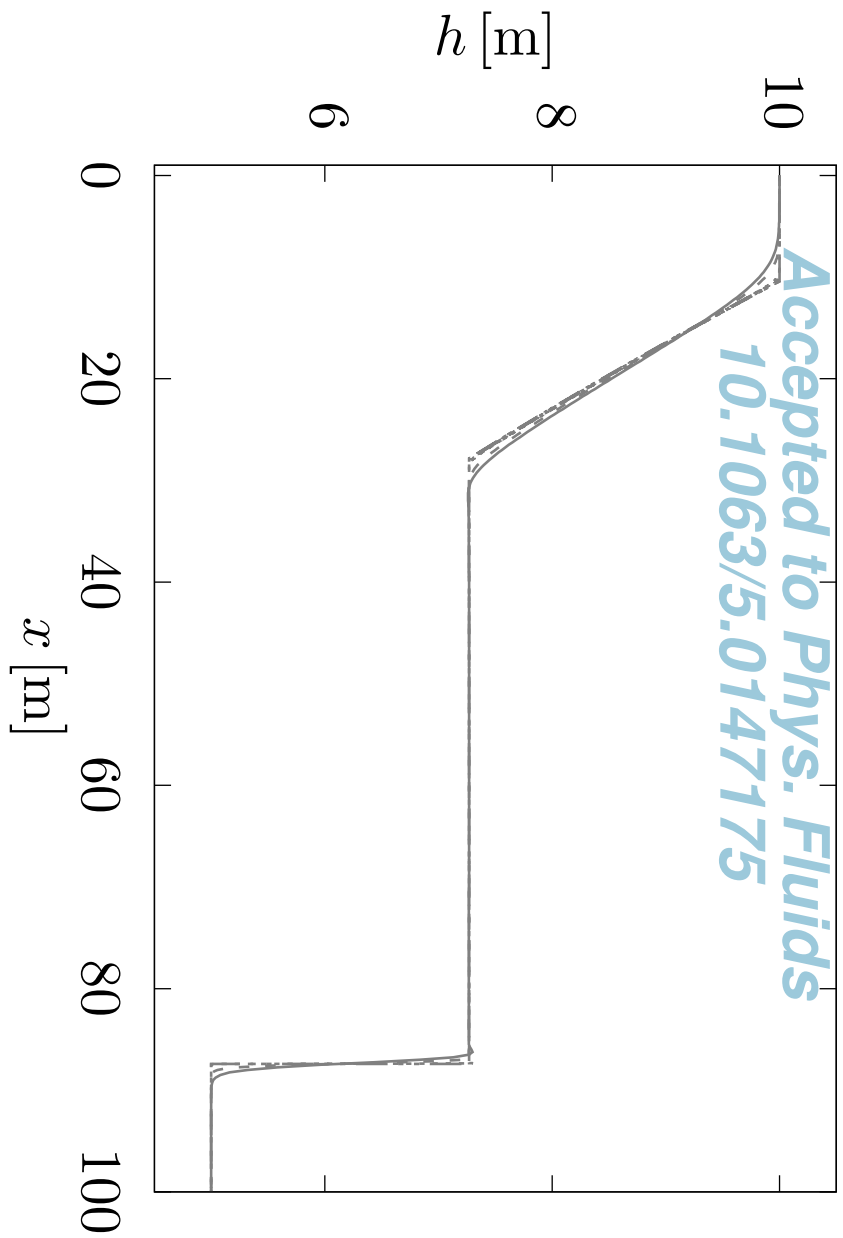

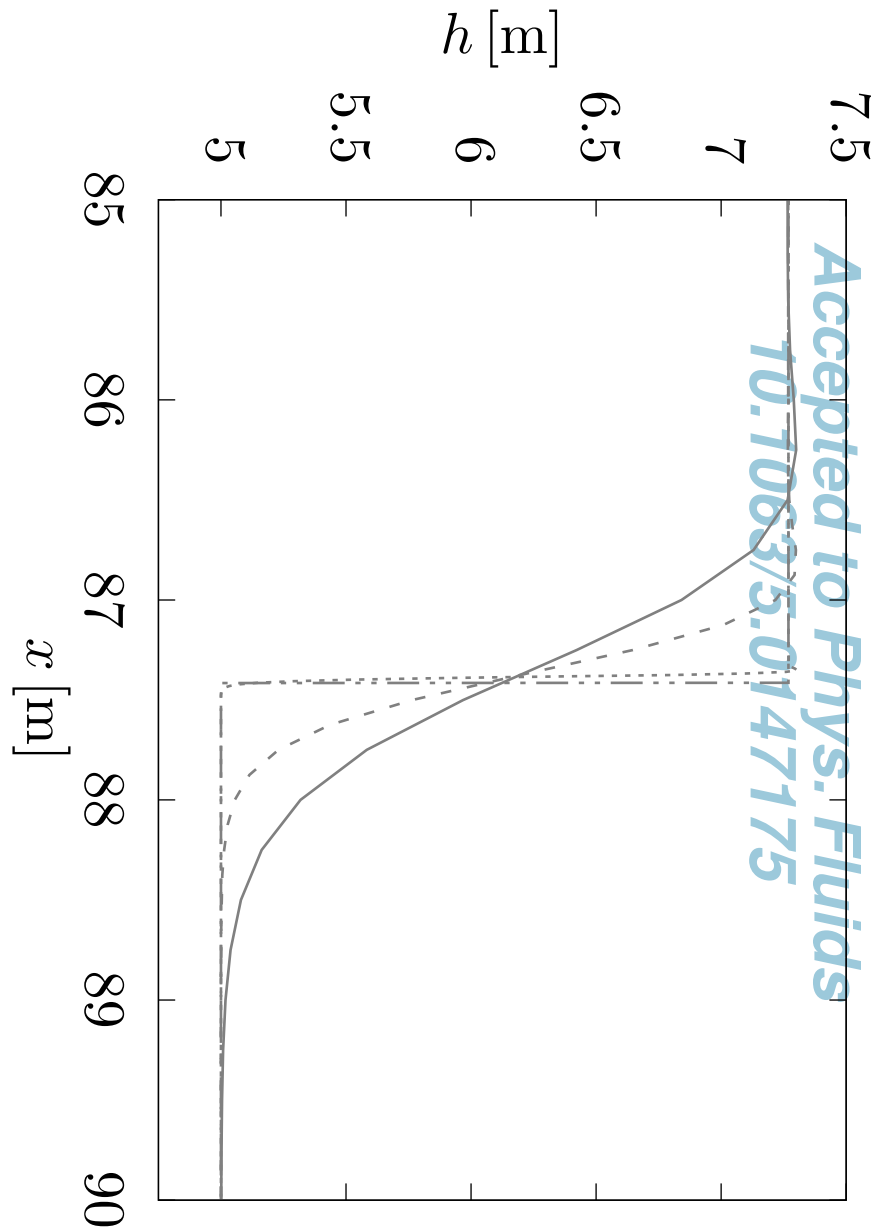

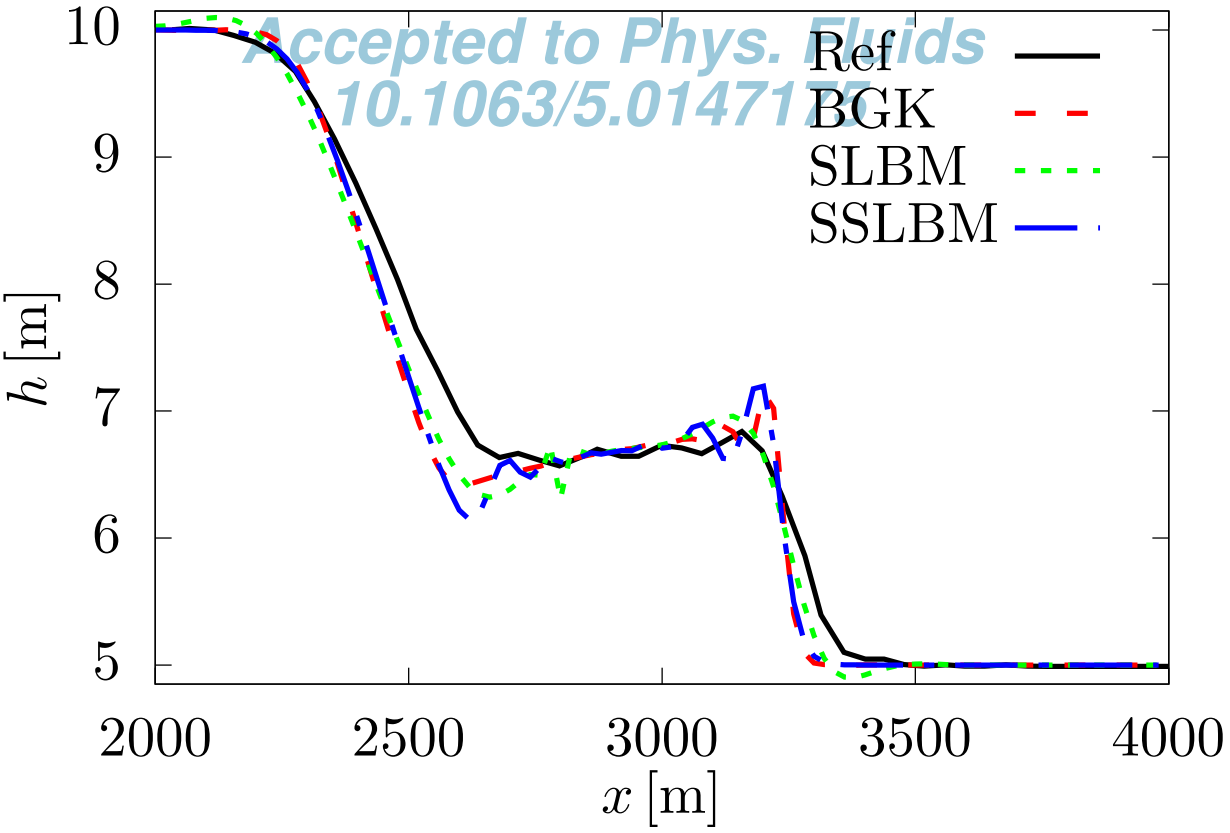

PLEASE CITE THIS ARTICLE AS DOI: 10.1063/5.0147175

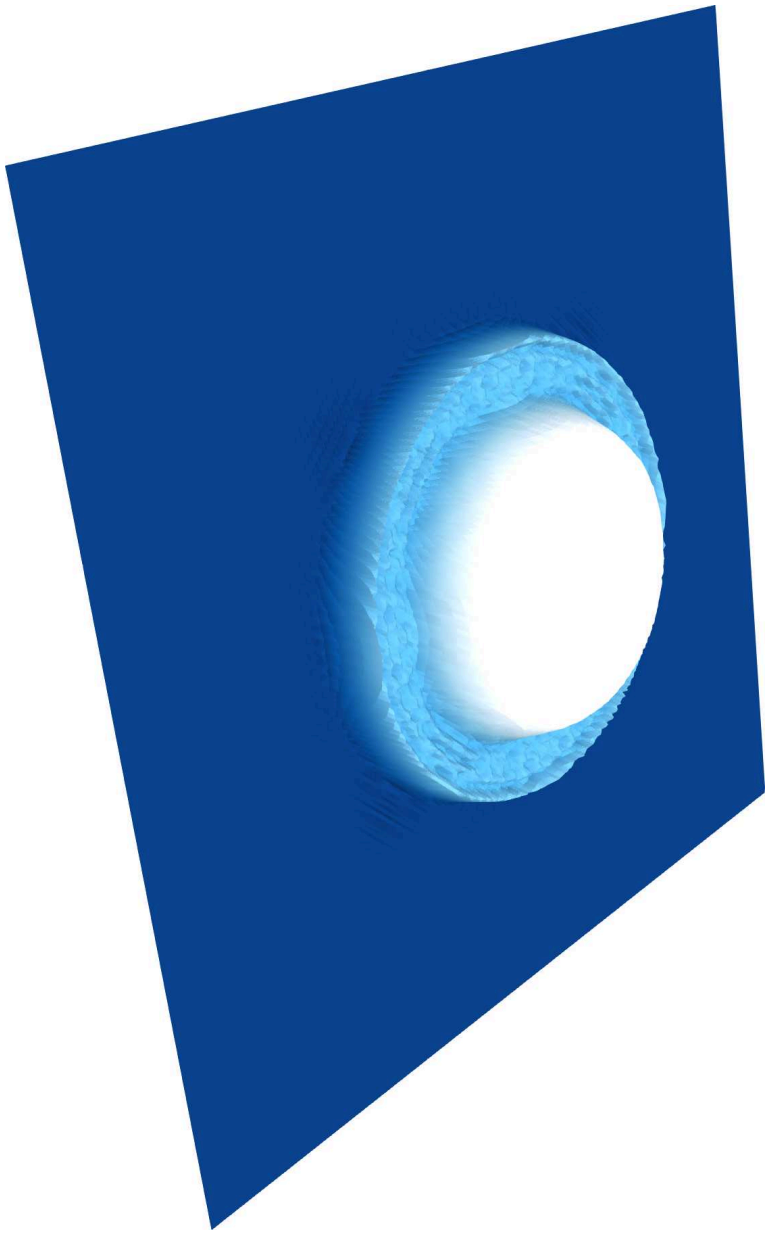

PLEASE CITE THIS ARTICLE AS DOI: 10.1063/5.0147175

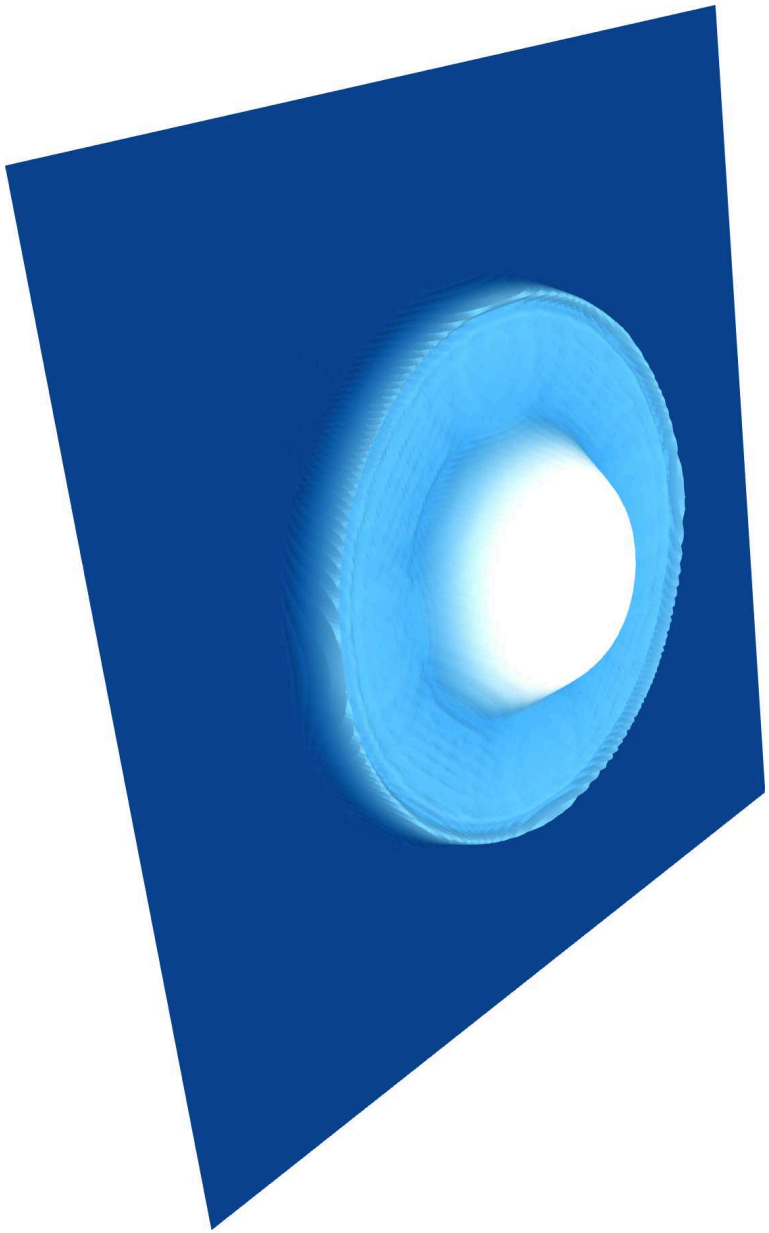

PLEASE CITE THIS ARTICLE AS DOI: 10.1063/5.0147175

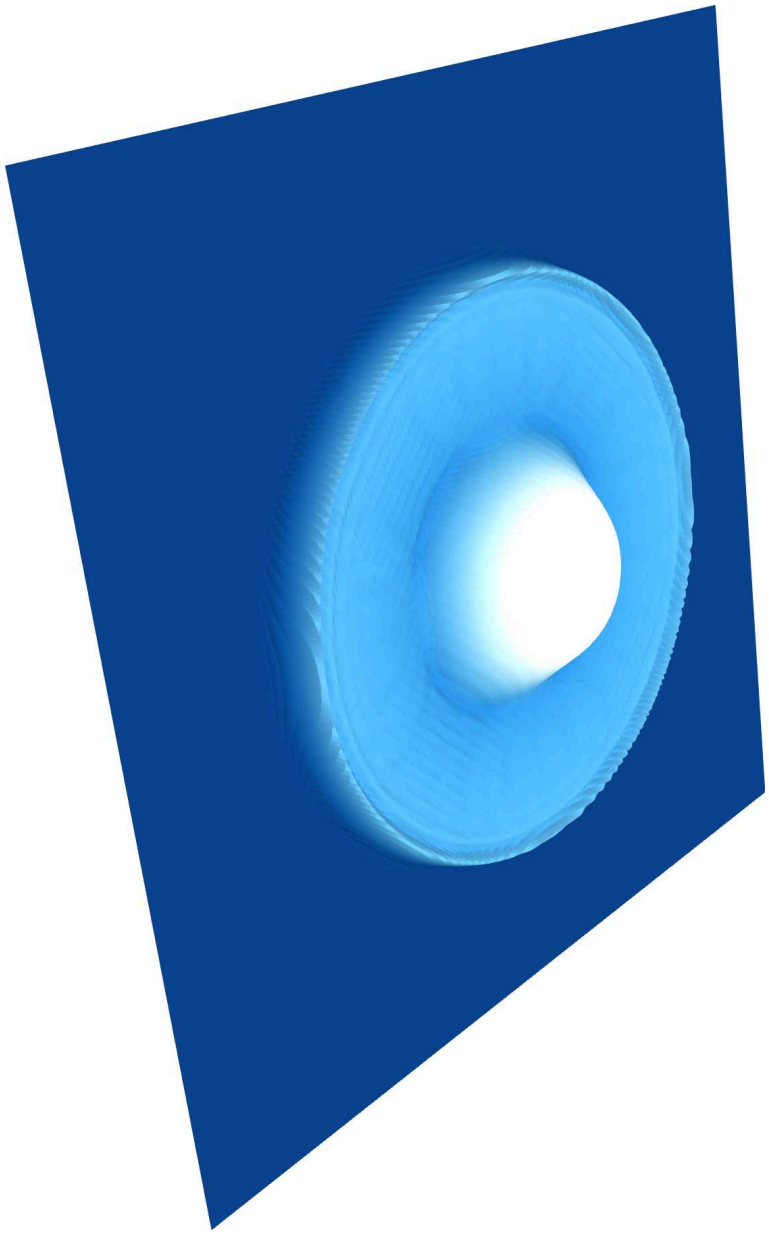

PLEASE CITE THIS ARTICLE AS DOI: 10.1063/5.0147175

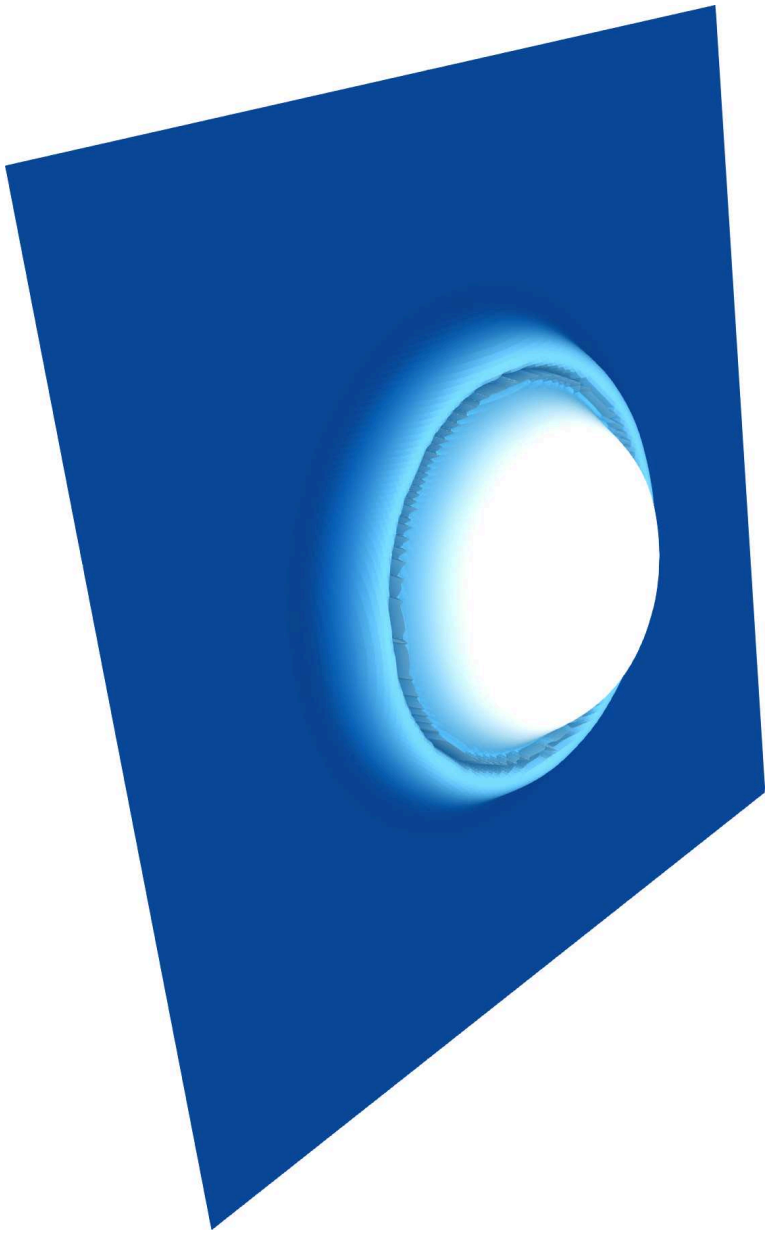

PLEASE CITE THIS ARTICLE AS DOI: 10.1063/5.0147175

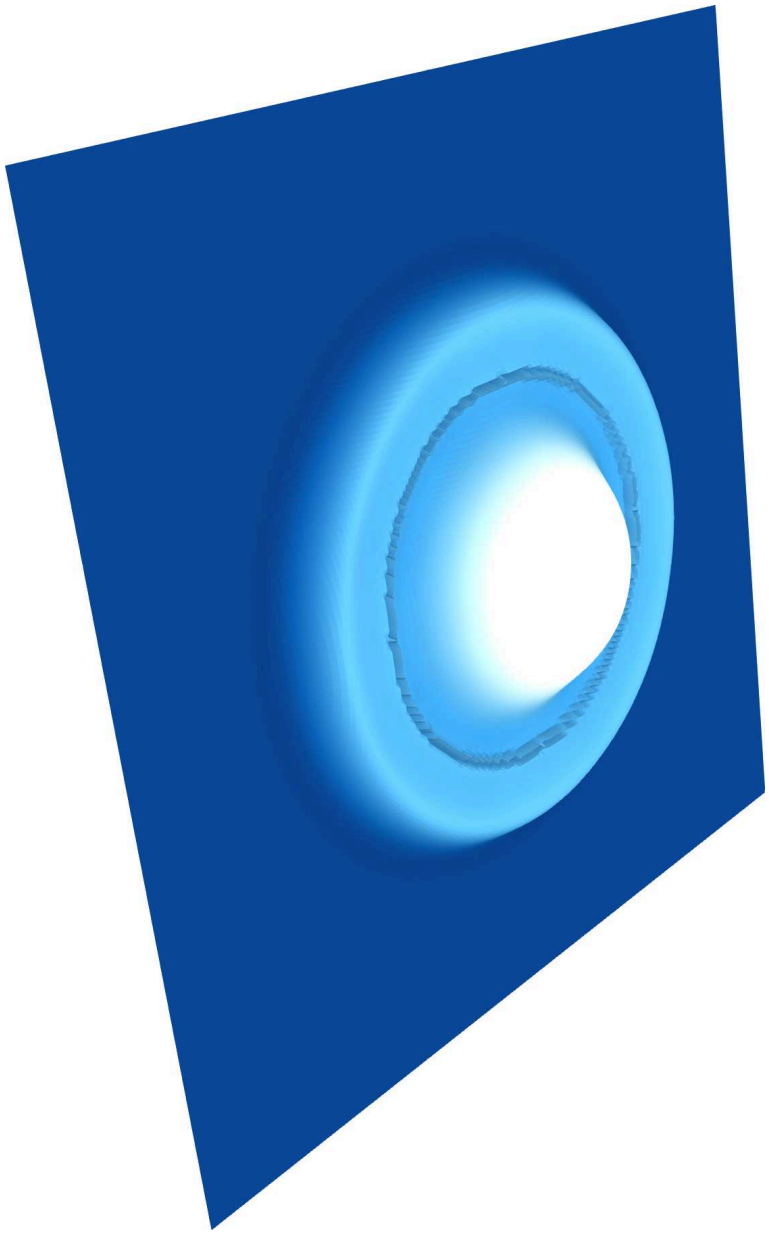

PLEASE CITE THIS ARTICLE AS DOI: 10.1063/5.0147175

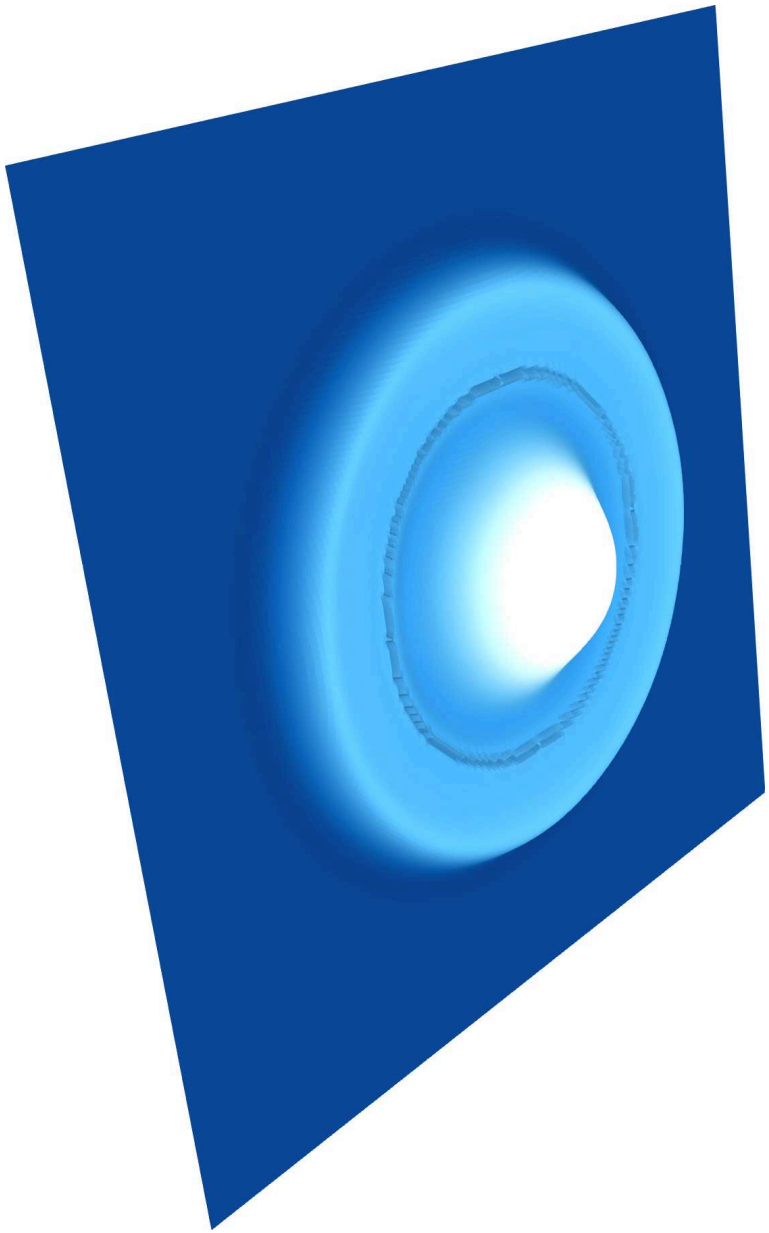

PLEASE CITE THIS ARTICLE AS DOI: 10.1063/5.0147175

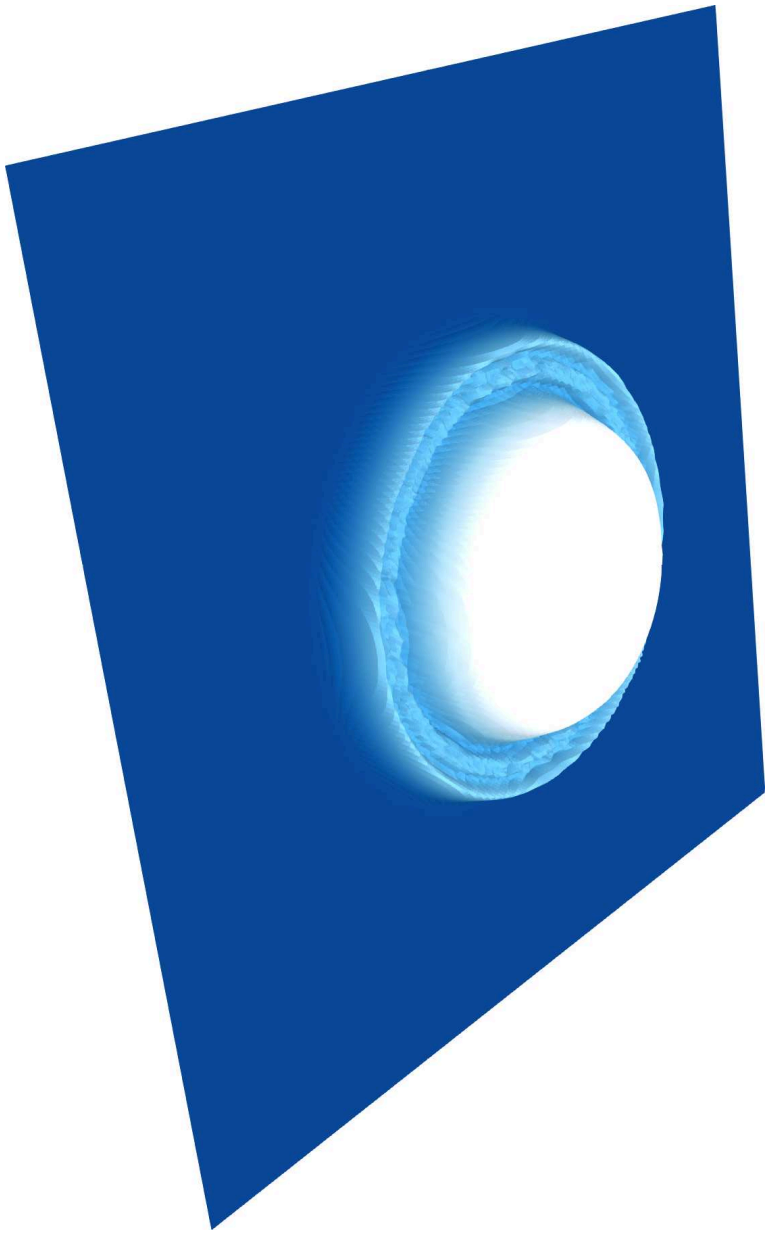

PLEASE CITE THIS ARTICLE AS DOI: 10.1063/5.0147175

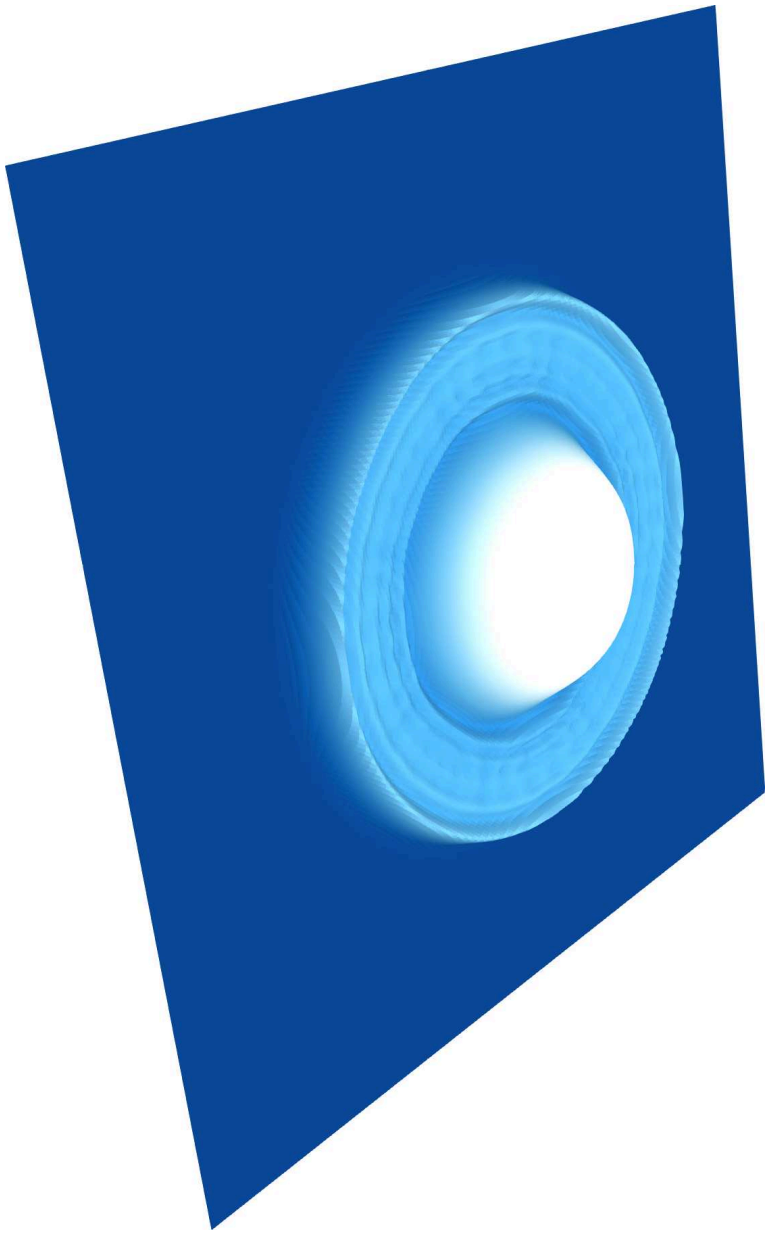

PLEASE CITE THIS ARTICLE AS DOI: 10.1063/5.0147175

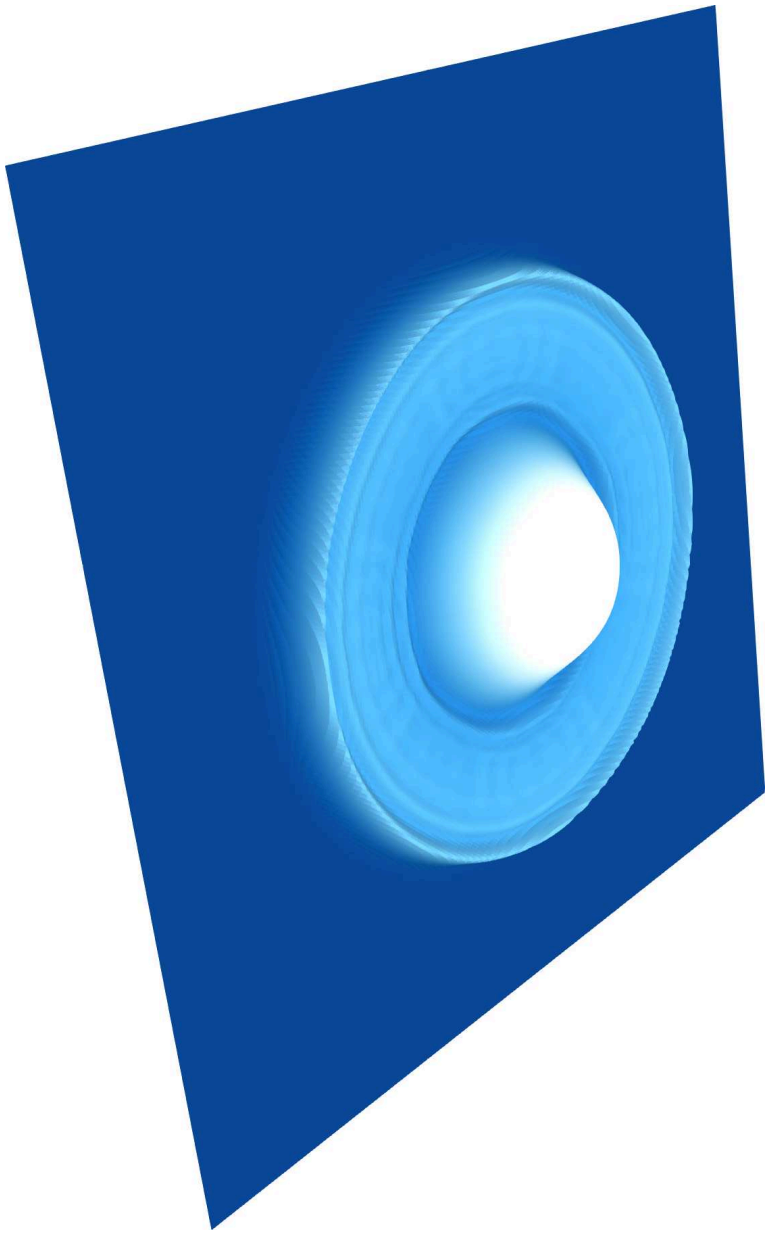

PLEASE CITE THIS ARTICLE AS DOI: 10.1063/5.0147175

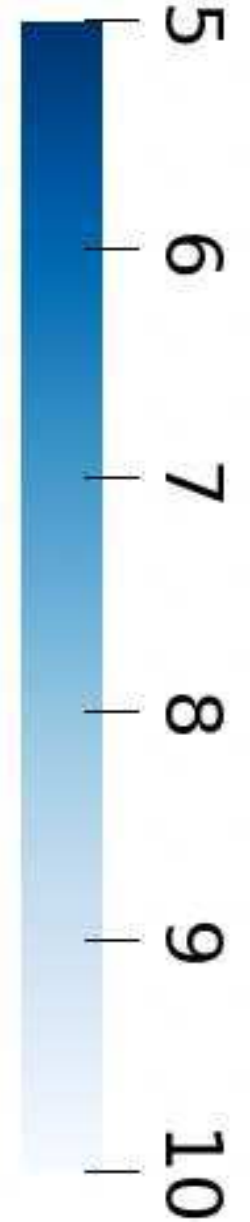

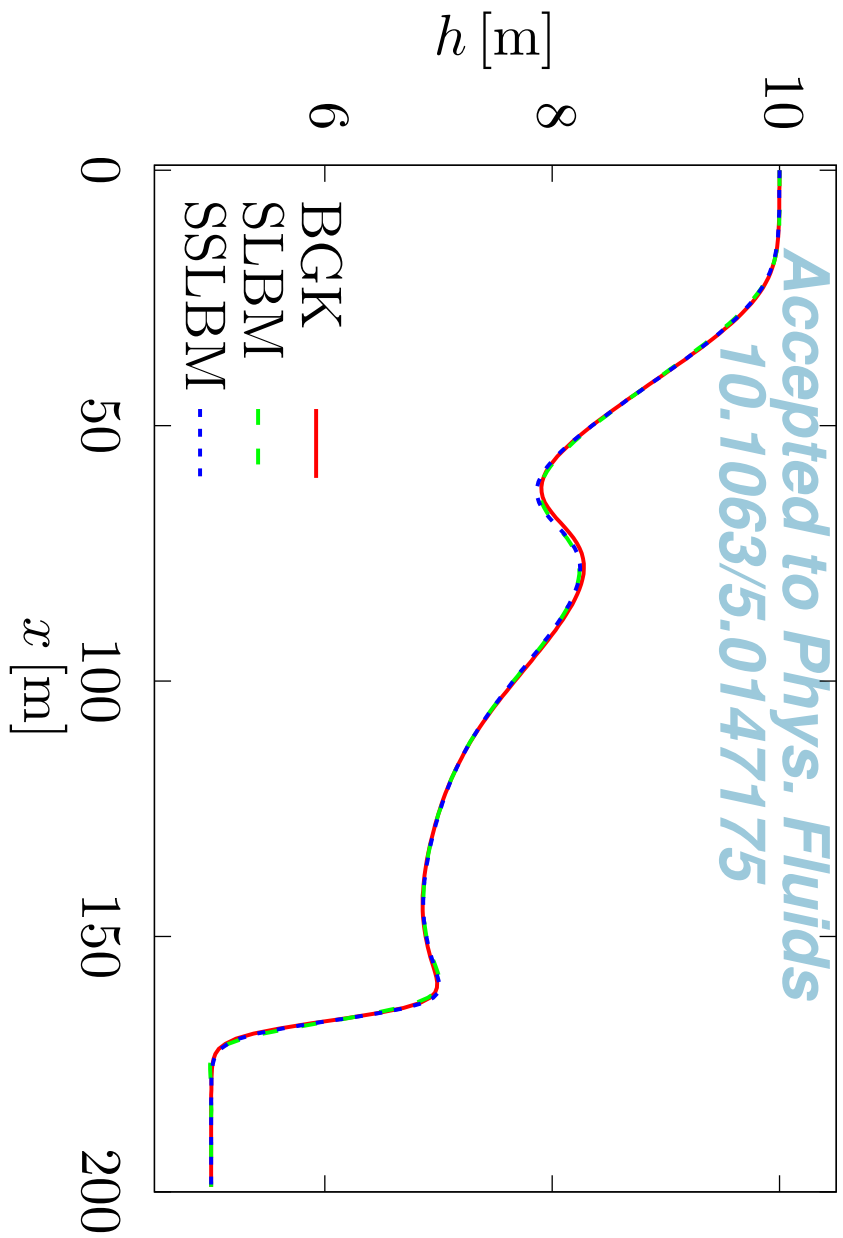

PLEASE CITE THIS ARTICLE AS DOI: 10.1063/5.0147175

PLEASE CITE THIS ARTICLE AS DOI: 10.1063/5.0147175

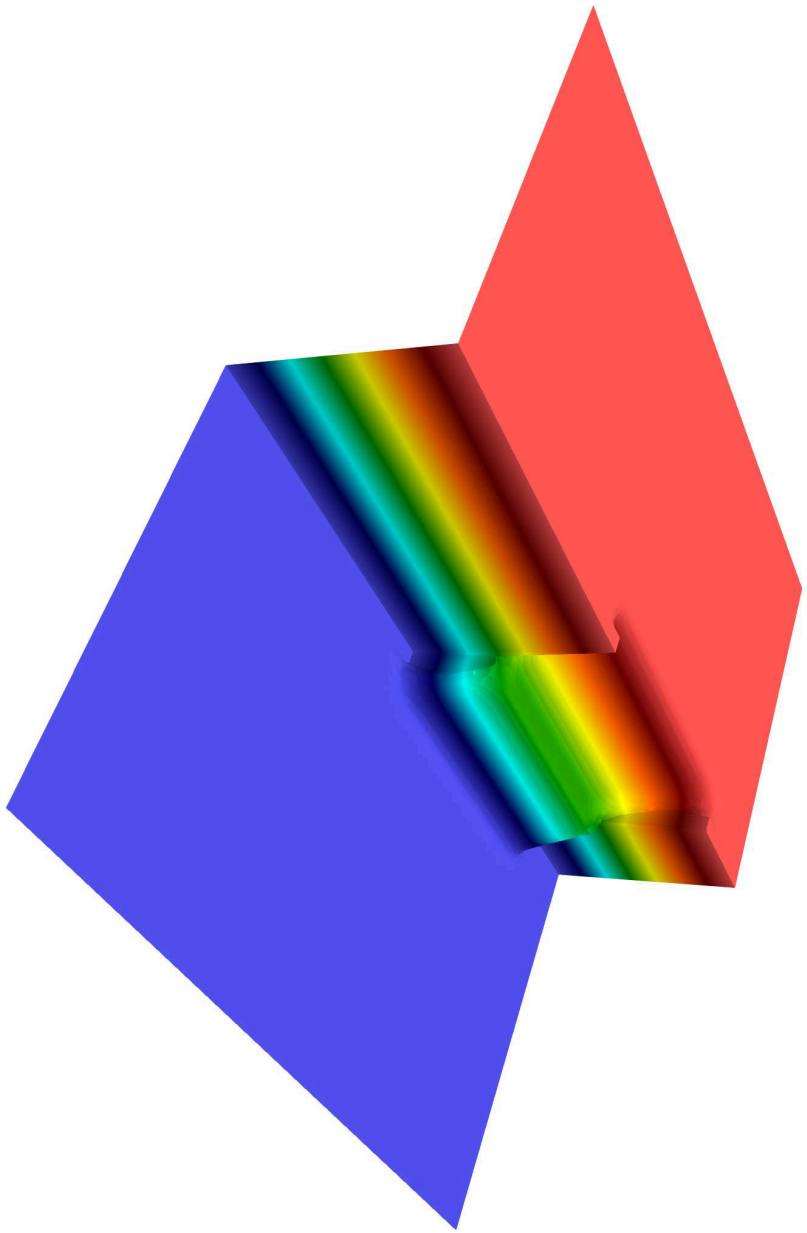

Physics of Fluids

PLEASE CITE THIS ARTICLE AS DOI: 10.1063/5.0147175

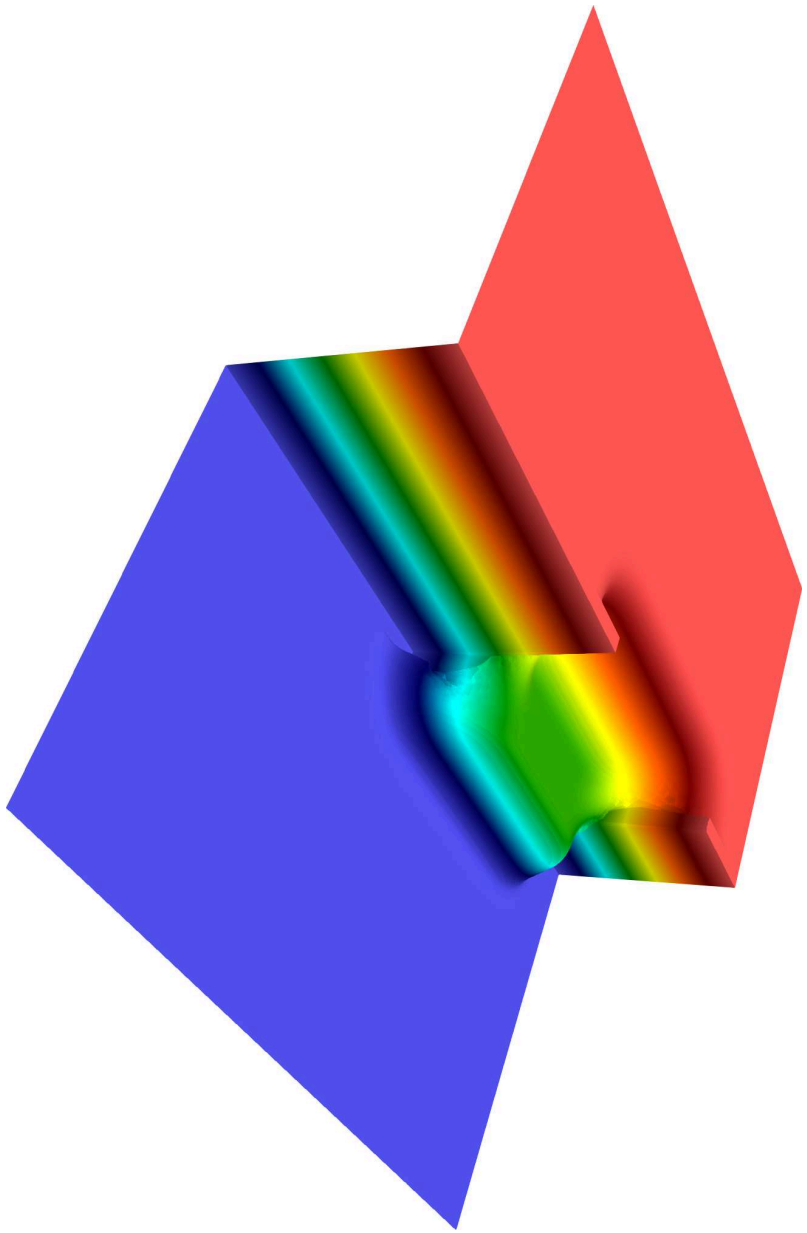

PLEASE CITE THIS ARTICLE AS DOI: 10.1063/5.0147175

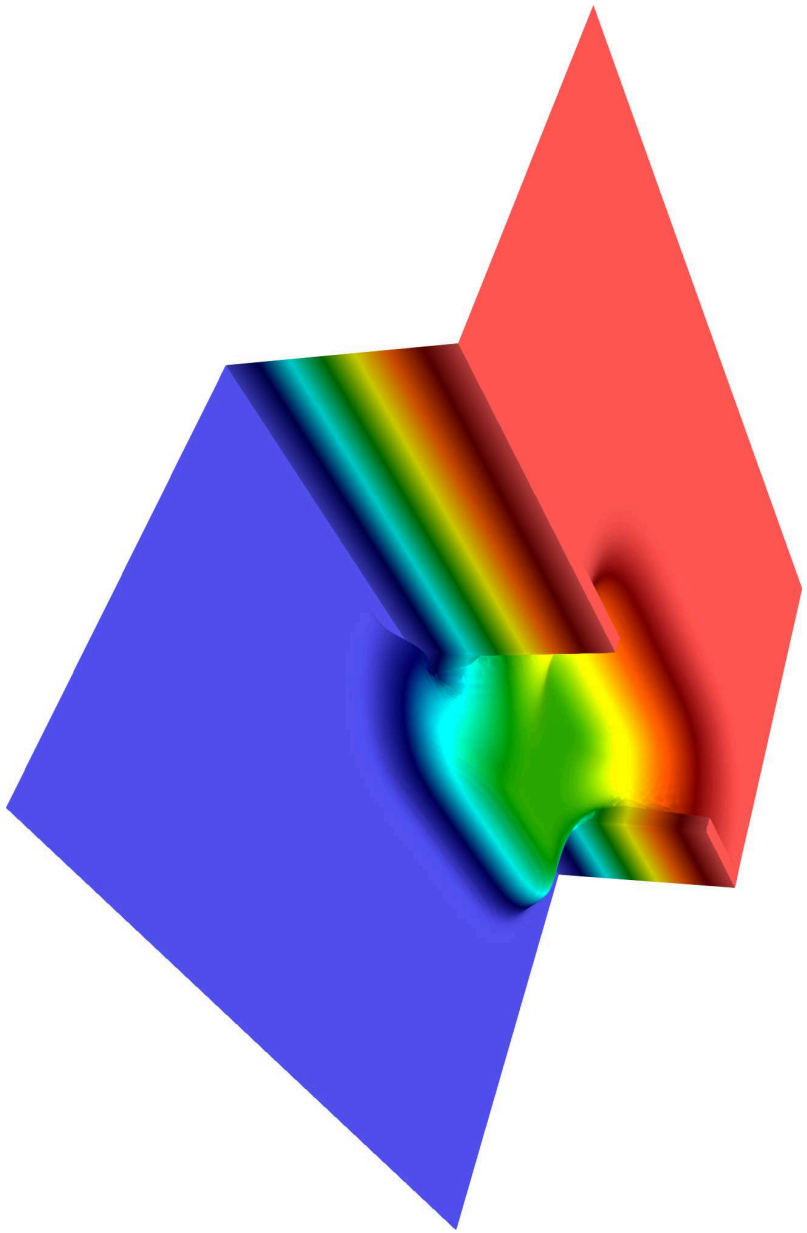

PLEASE CITE THIS ARTICLE AS DOI: 10.1063/5.0147175

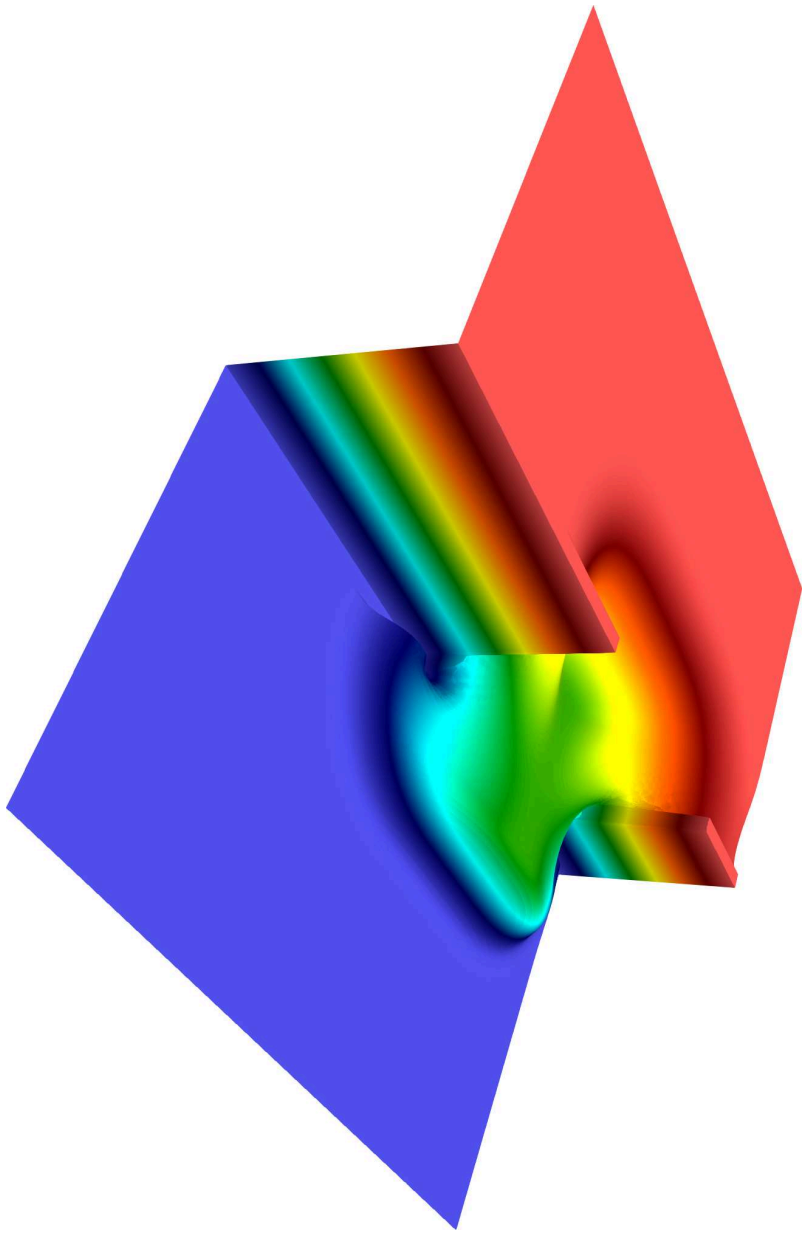

PLEASE CITE THIS ARTICLE AS DOI: 10.1063/5.0147175

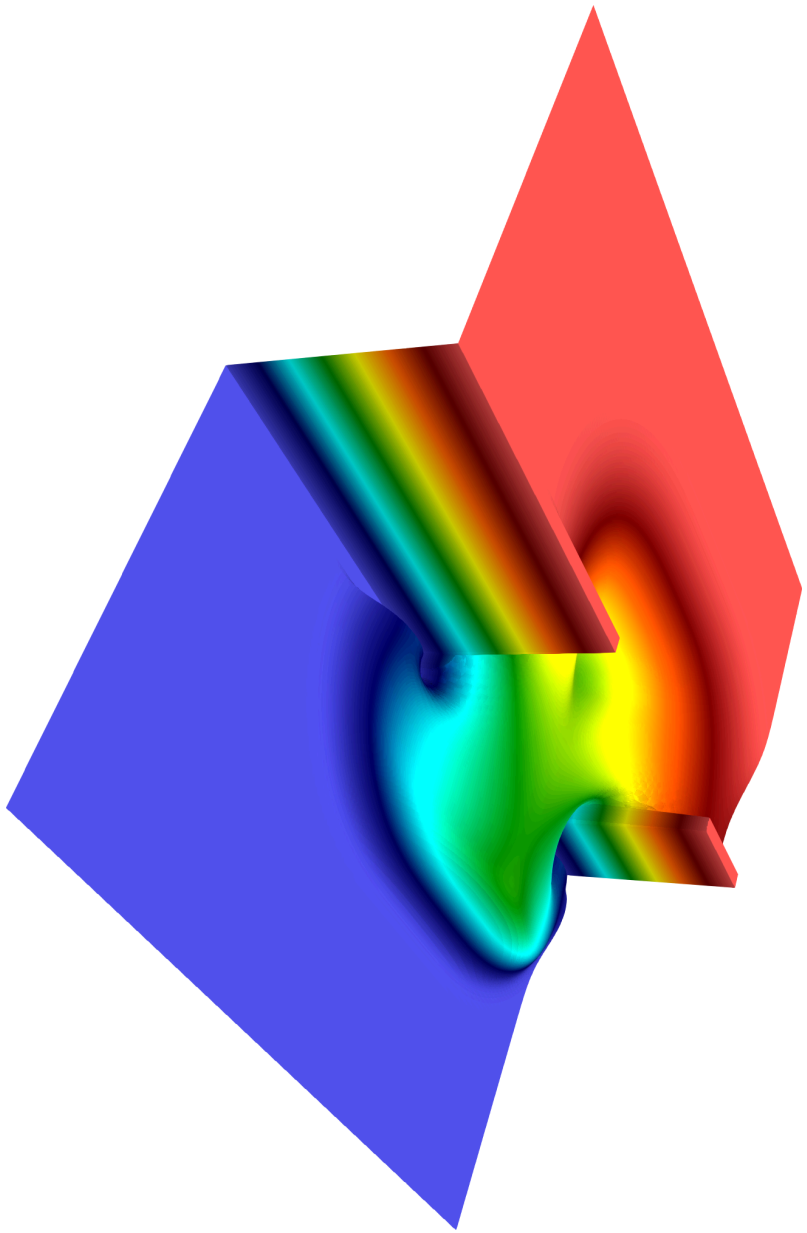

Physics of Fluids

PLEASE CITE THIS ARTICLE AS DOI: 10.1063/5.0147175

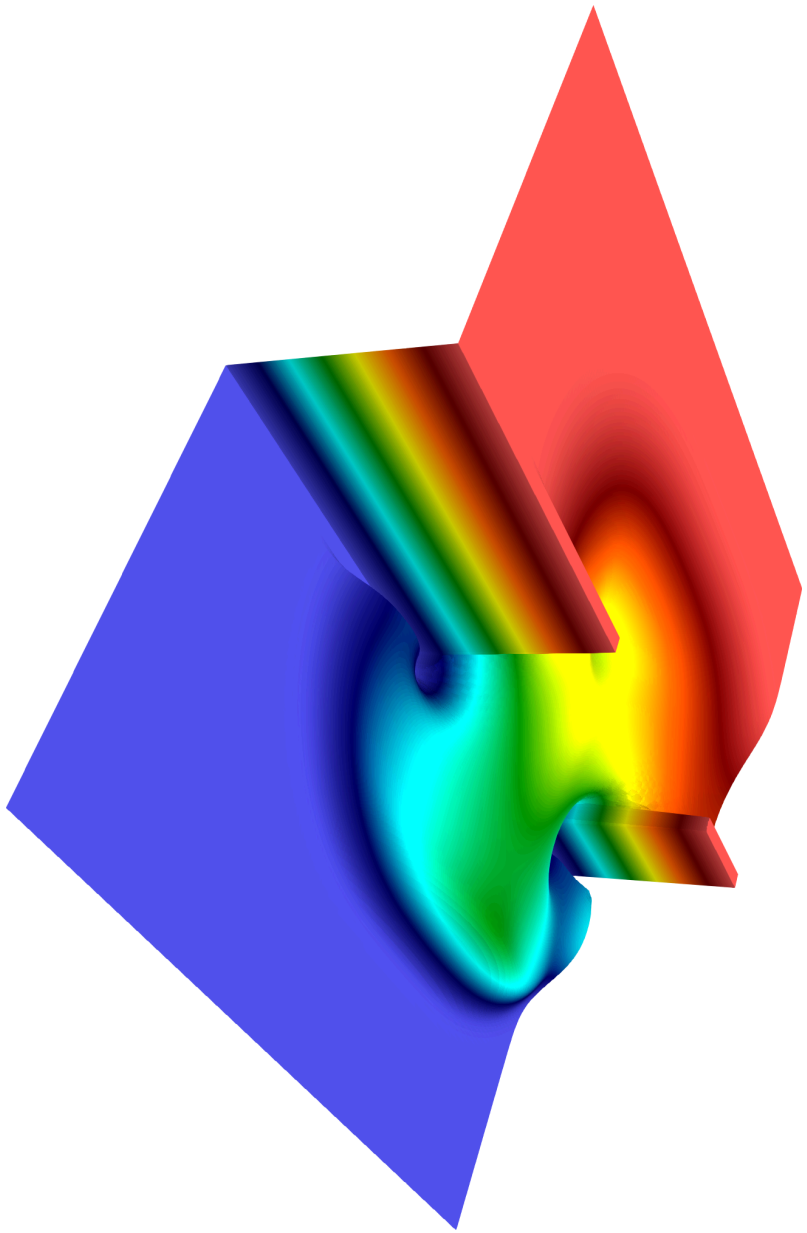

Physics of Fluids

PLEASE CITE THIS ARTICLE AS DOI: 10.1063/5.0147175

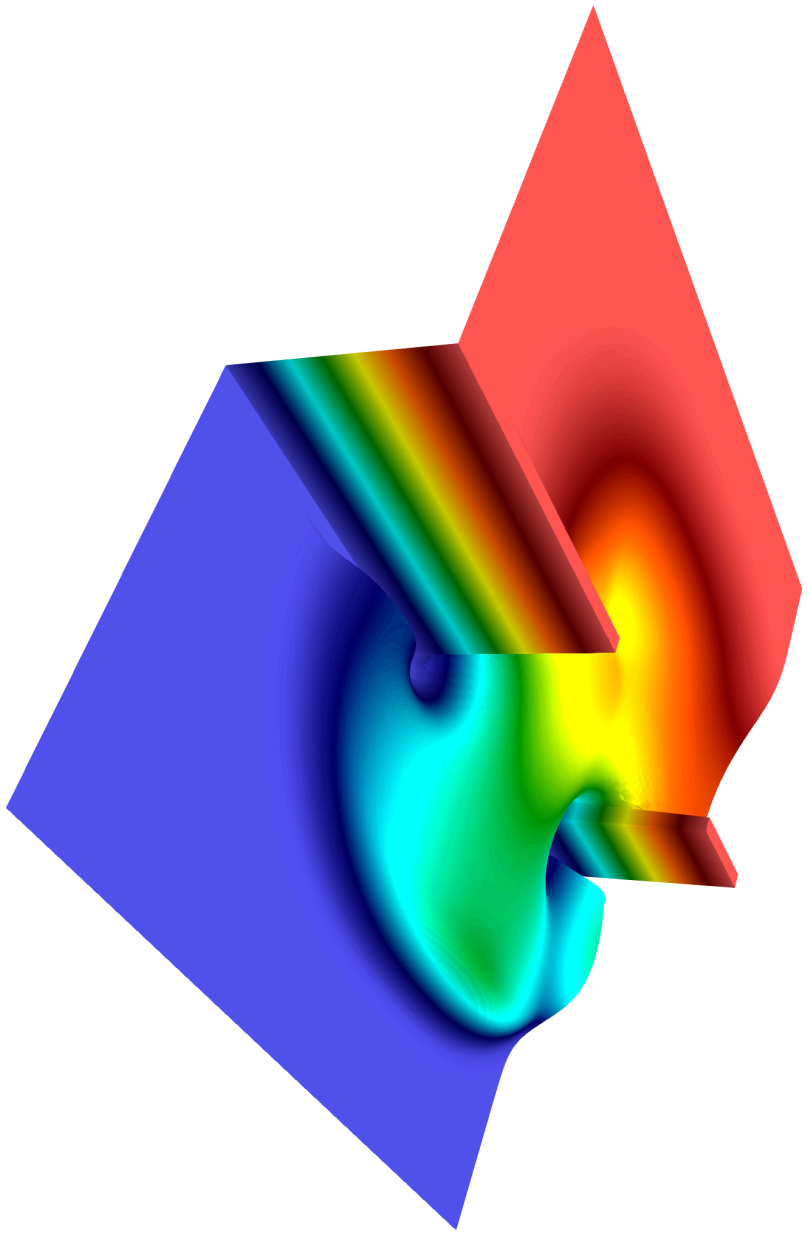

PLEASE CITE THIS ARTICLE AS DOI: 10.1063/5.0147175